AMERICAN SOCIETY FOR MICROBIOLOGY | Journal of Virology®

VACCINES AND ANTIVIRAL AGENTS

The XPB Subunit of the TFIIH Complex Plays a Critical Role in HIV-1 Transcription, and XPB Inhibition by Spironolactone Prevents HIV-1 Reactivation from Latency

Luisa Mori,[a] Katharine Jenike,[b] Yang-Hui Jimmy Yeh,[b] Benoît Lacombe,[c] Chuan Li,[a] Adam J. Getzler,[a] Sonia Mediouni,[a] Michael E. Cameron,[a] Matthew E. Pipkin,[a] Ya-Chi Ho,[b] Bertha Cecilia Ramirez,[c]* Susana T. Valente[a]

[a]The Scripps Research Institute, Department of Immunology and Microbiology, Jupiter, Florida, USA
[b]Department of Microbial Pathogenesis, Yale University School of Medicine, New Haven, Connecticut, USA
[c]Institut Cochin, INSERM, CNRS, Université Sorbonne Paris Cité, Paris, France

Katharine Jenike and Yang-Hui Jimmy Yeh contributed equally to this work; Bertha Cecilia Ramirez and Susana Valente contributed equally to this work.

ABSTRACT Human immunodeficiency virus (HIV) transcription requires assembly of cellular transcription factors at the human immunodeficiency virus type 1 (HIV-1) promoter. The TFIIH general transcription factor facilitates transcription initiation by opening the DNA strands around the transcription start site and phosphorylating the C-terminal domain of RNA polymerase II (RNAPII) for activation. Spironolactone (SP), an FDA approved aldosterone antagonist, triggers the proteasomal degradation of the XPB subunit of TFIIH and concurrently suppresses acute HIV infection *in vitro*. Here, we investigated SP as a possible block-and-lock agent for a functional cure, aimed at the transcriptional silencing of the viral reservoir. The long-term activity of SP was investigated in primary and cell line models of HIV-1 latency and reactivation. We show that SP rapidly inhibits HIV-1 transcription by reducing RNAPII recruitment to the HIV-1 genome. Short hairpin RNA (shRNA) knockdown of XPB confirmed XPB loss as the mechanism of action of HIV inhibition. Unfortunately, long-term pretreatment with SP does not result in long-term epigenetic suppression of HIV upon SP treatment interruption, since the virus rapidly rebounds when XPB reemerges; however, SP alone without antiretroviral therapy (ART) maintains transcriptional silencing of HIV. Importantly, SP inhibits HIV reactivation from latency in both cell line models and resting $CD4^+$ T cells isolated from aviremic individuals living with HIV upon cell stimulation with latency-reversing agents. Furthermore, long-term treatment with concentrations of SP that potently degrade XPB does not lead to global dysregulation of cellular mRNA expression. Overall, these results suggest that XPB plays a key role in HIV transcriptional regulation, and XPB degradation by SP strengthens the potential of HIV transcriptional inhibitors in block-and-lock cure approaches.

IMPORTANCE Antiretroviral therapy (ART) effectively reduces an individual's HIV loads to below the detection limit; nevertheless, rapid viral rebound immediately ensues upon treatment interruption. Furthermore, virally suppressed individuals experience chronic immune activation from ongoing low-level viral expression. Thus, the importance of identifying novel therapeutics to explore in block-and-lock HIV functional cure approaches, aimed at the transcriptional and epigenetic silencing of the viral reservoir to block reactivation from latency, is apparent. We investigated the potential of repurposing the FDA-approved spironolactone (SP) as one such drug. SP treatment rapidly degrades a host transcription factor subunit, XPB, inhibiting HIV transcription and blocking reactivation from latency. Long-term SP treatment does not affect cellular viability, cell cycle progression, or global cellular transcription. SP alone blocks HIV transcription in the absence of ART but does not delay rebound upon

Citation Mori L, Jenike K, Yeh Y-HJ, Lacombe B, Li C, Getzler AJ, Mediouni S, Cameron ME, Pipkin ME, Ho Y-C, Ramirez BC, Valente ST. 2021. The XPB subunit of the TFIIH complex plays a critical role in HIV-1 transcription, and XPB inhibition by spironolactone prevents HIV-1 reactivation from latency. J Virol 95:e01247-20. https://doi.org/10.1128/JVI.01247-20.

Editor Guido Silvestri, Emory University

Address correspondence to Bertha Cecilia Ramirez, cecilia.ramirez@i2bc.paris-saclay.fr, or Susana T. Valente, svalente@scripps.edu.

* Present address: Bertha Cecilia Ramirez, Institute for Integrative Biology of the Cell (I2BC), CEA, CNRS, Université Paris-Sud, Université Paris-Saclay, Gif-sur-Yvette, Paris, France.

Received 22 June 2020
Accepted 11 November 2020
Accepted manuscript posted online 25 November 2020
Published 28 January 2021

drug removal, as XPB rapidly reemerges. This study highlights XPB as a novel drug target in block-and-lock therapeutic approaches.

KEYWORDS block-and-lock, HIV transcription, spironolactone, TFIIH, XPB, inhibition

Upon human immunodeficiency virus type 1 (HIV-1) integration into the host genome, the provirus becomes transcriptionally silent as the cell returns to a quiescent state (1). Despite effective antiretroviral therapy (ART) that suppresses HIV-1 replication to below the detection limit, these latent proviruses can reinitiate viral production upon cell stimulation or treatment interruption (2–4). The total elimination of this latent reservoir has become a major goal of HIV-1 eradication strategies, and interventions involving latency modifying agents, immune therapies, or gene and cell-based therapies are being investigated (5–7). More recently though, HIV-1 remission or a functional cure have been explored (8, 9). A functional cure entails either null or sufficiently low viral replication that is controlled by the immune system in the absence of ART, while proviral DNA remains detectable. This would allow the prospect of functionally cured individuals maintaining undetectable viral loads in the absence of ART without risk of onward transmission and no ongoing immunological damage that is associated with HIV infection (10–12). One such functional cure approach has been branded the block-and-lock approach, which aims at the transcriptional silencing of the viral reservoir (5). There are unfortunately no clinically available HIV-1-specific transcriptional inhibitors.

Transcription at the HIV-1 promoter begins with the assembly of the preinitiation complex (PIC). The 5′ long terminal repeat (LTR), which serves as the viral promoter, contains binding sites for multiple transcription factors (TFs), which bind sequentially to form the PIC. These include NF-κB, Sp1, TATA-binding protein (TBP) (as part of the general transcription factor TFIID), TFIIA, TFIIB, and TFIIF, which together direct RNA polymerase II (RNAPII) binding to form a stable promoter complex (13–15). The PIC is completed by the addition of the TFIIE heterodimer and TFIIH (15). TFIIH is a 10-protein complex consisting of a core (XPB, XPD, p62, p52, p44, p34, and p8) and cyclin-dependent kinase (CDK)-activating kinase (CAK) subcomplex (CDK7, cyclin H, and MAT1) (16). TFIIH plays a crucial role in the initiation of transcription but also in nucleotide excision repair, where bulky adducts are removed from damaged DNA (17). In transcription, once the PIC has assembled, the XPB subunit functions as a DNA translocase, feeding the DNA into the RNAPII cleft, introducing negative supercoiling, and initiating the formation of the transcription bubble (16, 18, 19). The CDK7 subunit is responsible for the initial activating phosphorylation of serine 5 in the heptapeptide repeats on the RNAPII (C-terminal domain [CTD]) tail (pSer5) (20–22). Activated RNAPII clears the promoter but rapidly stalls after transcribing the first ~59 nucleotides downstream of the transcription start site (TSS), which comprises a secondary structure termed the transactivation response element (TAR) (23). RNAPII stalls for a few reasons, namely, its association with negative elongation factors, NELF and DSIF, as well as the presence of nucleosome 1 (Nuc-1) downstream from the TSS that occlude efficient elongation (24–26). The high-affinity interaction of the viral protein Tat, which is produced from rare full-length transcripts, with the TAR RNA allows recruitment of the positive elongation factor, P-TEFb, consisting of cyclin T1 and CDK9 (24, 25, 27–33). CDK9 phosphorylation of NELF (leading to detachment from RNAPII), DSIF (converts to an elongation factor), as well as Ser2 on the RNAPII CTD allows transcription to proceed (34, 35). Tat plays a fundamental role in HIV transcription and is key for the rapid and robust increase in full-length viral transcripts from the HIV genome upon reactivation from latency (28, 36–39). The proof-of-concept for the block-and-lock approach was shown with the small-molecule inhibitor of Tat, didehydro-cortistatin A (dCA) in $CD4^+$ T cells isolated from infected individuals and in the humanized mouse model of HIV latency (40–42). dCA directly interacts with the basic domain of Tat, blocking the interaction of Tat with TAR and preventing transcriptional elongation (40). As such, the long-term treatment of cells with dCA restricts RNAPII recruitment to the promoter, and over time

epigenetic marks are deposited at the HIV-1 promoter, promoting silencing and blocking reactivation from latency (41, 43, 44).

In search for novel molecules that regulate HIV transcription to increase our portfolio of block-and-lock agents, we studied the action of spironolactone (SP). SP is a potassium-sparing diuretic, an aldosterone antagonist that blocks binding to the mineralocorticoid receptor (MR), and has been approved since 1959 for the treatment of a range of conditions, including hypertension and heart failure (45). An off-target effect of SP is the proteasomal degradation of the ATP-dependent helicase, XPB subunit of the transcription factor TFIIH complex (46–49). XPB degradation is dependent on the 26S proteasome and ubiquitinating enzymes (46). SP triggers XPB Ser90 phosphorylation by the CDK7 subunit of TFIIH leading to SCF^{FBXL18} E3 ligase-mediated ubiquitination and proteasomal degradation (50). Despite XPB's critical role in transcription initiation (14, 16), its degradation was reported not to affect global transcription (51, 52). However, subsequent studies showed transcriptional inhibition of genes highly dependent on NF-κB (47, 51). The two binding sites for NF-κB at the HIV-1 LTR allow NF-κB control of HIV-1 reemergence from latency (53). Lacombe et al. previously demonstrated that XPB degradation, by short-term treatment of cells with SP, inhibits acute HIV-1 and HIV-2 transcription (48).

Here, we explored the potential of SP as a block-and-lock agent through long-term treatment of latently infected cells and resting $CD4^+$ T cells explanted from infected individuals. We demonstrated the ability of SP to inhibit HIV-1 transcription in latently infected cells and suppress reactivation from latency by potent latency reversing agents (LRAs), which correlated with loss of RNAPII recruitment to the HIV-1 promoter and genome, without damaging cellular effects. We confirmed that the activity of SP was mediated by XPB via knockdown studies and is independent of the Tat-TAR interaction. Altogether, our results suggest that XPB plays a key role in HIV-1 transcriptional activation, and its inhibition by SP blocks HIV-1 expression.

RESULTS

Treatment of latently infected cell lines with SP inhibits transcription of HIV-1. SP has been previously shown to block acute HIV infection of $CD4^+$ T cells (48). Here, to explore whether SP could be used in block-and-lock approaches to an HIV cure, we investigated its ability to inhibit HIV-1 transcription in cell line models of latency. We studied SP activity in two established cell line models of latency, OM-10.1 and ACH-2 cells, in the presence of ART. OM-10.1 cells are a promyelocytic line derived from HL-60 cells that survived an acute HIV-1 infection. Each cell contains a single integrated, full-length provirus (54). SP treatment of these cells resulted in a dose-dependent reduction of HIV-1 capsid p24 in the supernatant, with a half-maximal inhibitory concentration (IC_{50}) of 1.77 μM (Fig. 1A). This inhibition correlated with a dose-dependent degradation of the cellular protein XPB (Fig. 1B). Eplerenone (EPL), a more selective mineralocorticoid receptor (MR) antagonist analog of SP, does not lead to XPB degradation (46, 47, 51, 55). As previously reported (48), no inhibition of HIV-1 was observed with increasing concentrations of EPL (Fig. 1C), suggesting that the mechanism of HIV-1 inhibition is independent of MR antagonism. No cytotoxicity was observed with up to 50 μM SP or EPL following a 72-h incubation (Fig. 1D).

Next, we evaluated the long-term effects of SP treatment. OM-10.1 cells were treated with 10 μM SP and 10 μM EPL or dimethyl sulfoxide (DMSO) for 190 days (Fig. 1E), and capsid p24 released into the supernatant was quantified by p24 enzyme-linked immunosorbent assay (ELISA). In OM-10.1 cells, SP rapidly inhibits viral production by approximately 2.5 logs, with capsid p24 levels stabilizing around the limit of detection (3 pg/ml). As expected, a reduction in the HIV-1 mRNA expression was observed in parallel (Fig. 1F, red line). The mRNA levels of the XPB gene, *ERCC3*, were either unaffected or slightly elevated by SP treatment (Fig. 1F, brown line). This confirms previous reports that degradation of XPB by SP is mediated by the 26S proteasome and not by reduced XPB mRNA expression (46). Of note, the half-life of SP in

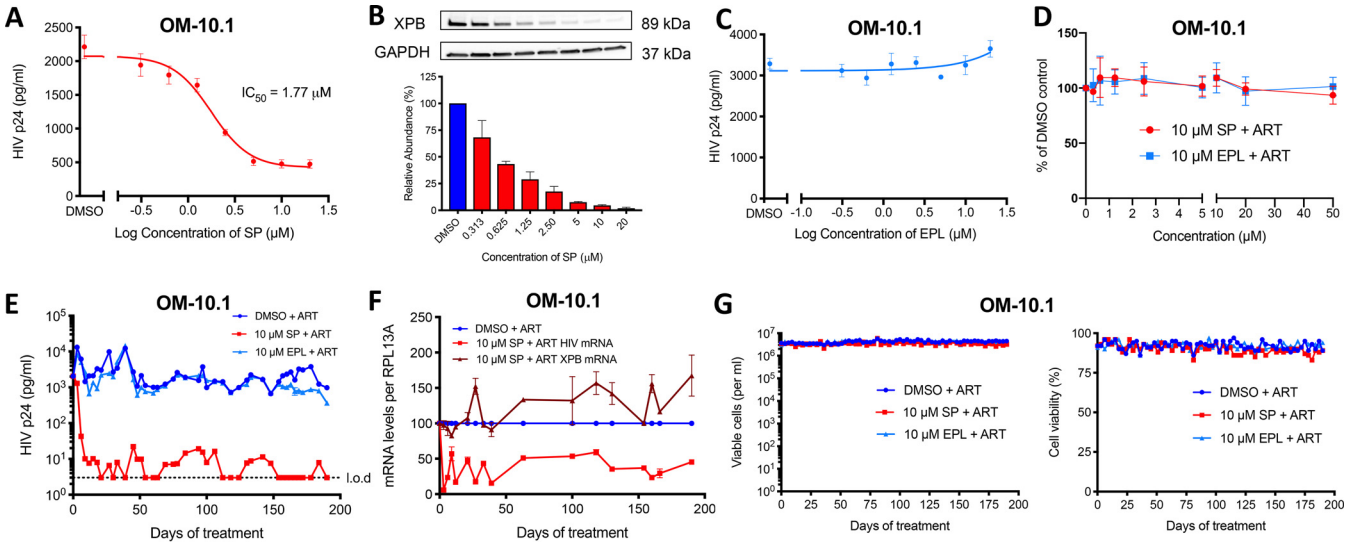

FIG 1 SP treatment inhibits latent HIV-1 transcription in the OM-10.1 cell line model of latency. (A) OM-10.1 cells were treated with ART and the indicated concentrations of SP for 72 h, after which the amount of HIV capsid was measured in the supernatant by p24 ELISA. The IC_{50} value was calculated using GraphPad Prism. The line represents the mean of three independent experiments, each with three technical replicates. Error bars represent SD. (B) Cells treated in panel A were collected for Western blotting analysis with the indicated antibodies. Protein abundance was calculated by normalization to GAPDH levels and plotted relative to the DMSO control. A representative blot is shown above the quantification of three independent experiments. Error bars represent SD. (C) OM-10.1 cells were treated with ART and the indicated concentrations of EPL for 72 h, and the IC_{50} values were calculated as in panel A. (D) Cytotoxicity of SP- (red) and EPL-treated (blue) cells in OM-10.1 cells treated for 72 h with increasing concentrations of SP was measured using an MTT assay and plotted as a percentage of the DMSO control. Error bars represent SD from three independent experiments. (E) OM-10.1 cells were split and treated every 72 h in the presence of ART with 10 μM SP (red), EPL (light blue), or vehicle only (DMSO, dark blue). HIV capsid production was quantified by p24 ELISA. The dotted black line at 3 pg/ml represents the limit of detection (LOD). This plot is representative of three independent experiments. (F) Cell-associated HIV mRNA levels (red) and *ERCC3* (XPB) mRNA levels (brown) were measured at multiple time points during the long-term treatments of OM-10.1 with 10 μM SP in panel E. cDNA was prepared from RNA extracted from cells pellets and qPCR performed with primers in the Nef region. The results were normalized as the number of viral mRNA copies per RPL13A mRNA and plotted relative to those of the DMSO-treated control (blue, set to 100% for each time point). Error bars represent SD from the qPCR. (G) The number of viable cells per milliliter of culture (left) and percentage viable cells (right), respectively, were measured by trypan blue staining and an automated cell counter every 72 h during the long-term treatments of OM-10.1 cells with 10 μM SP, 10 μM EPL, or DMSO only.

long-term culture of OM-10.1 cells with ART was determined by liquid chromatography-tandem mass spectrometry (LC-MS/MS) to be 2.3 ($\pm$0.2) days, and cells were split and treated every 3 days. All experiments were performed in the presence of ART unless otherwise stated. Of note, without ART the half-life is 2.9 ($\pm$1.7) days. Altogether, these results suggest that, in OM-10.1 cells, SP treatment combined with ART over time inhibits HIV-1 transcription to very low, frequently undetectable levels without obvious cytotoxic effects in the cells.

We next assessed the activity of SP in the ACH-2 cell line, a T cell clone containing a single integrated provirus (56, 57), which harbors a C37T mutation TAR such that the Tat-TAR feedback loop is defective, resulting in low transcription rates (58, 59). SP treatment of these cells resulted in a similar dose-dependent reduction of HIV-1 capsid p24 in the supernatant, with an IC_{50} of 1.95 μM (Fig. 2A), which correlated with a dose-dependent degradation of XPB (Fig. 2B). Again, EPL was inactive against HIV (Fig. 2C). Cytotoxicity was not observed for up to 20 μM SP for a 72-h period or up to 50 μM with EPL (Fig. 2D). The long-term treatment of ACH-2 cells inhibited viral production by 1 to 1.5 logs, with capsid production stabilizing around 20 to 100 pg/ml (Fig. 2E). As expected, a reduction in cell-associated HIV RNA was also observed (Fig. 2E), while levels of XPB mRNA were either unaffected or slightly elevated (Fig. 2F). No difference in cell viability or cell number was observed over time (Fig. 2G). Differences in the magnitude of SP activity on HIV-1 p24 production between OM-10.1 and ACH-2 cells may be related to the level of XPB degradation in these cell lines, 95% in OM-10.1 cells compared to 81% in ACH-2 cells (Fig. 1B and 2B). Given that SP inhibits the transcription from proviruses with an incompetent Tat-TAR feedback loop, as is the case for ACH-2 cells, the mechanism of action of SP is likely independent of the Tat-TAR interaction.

We also investigated the potential of SP to inhibit SIVmac239 in HUT-78 cells.

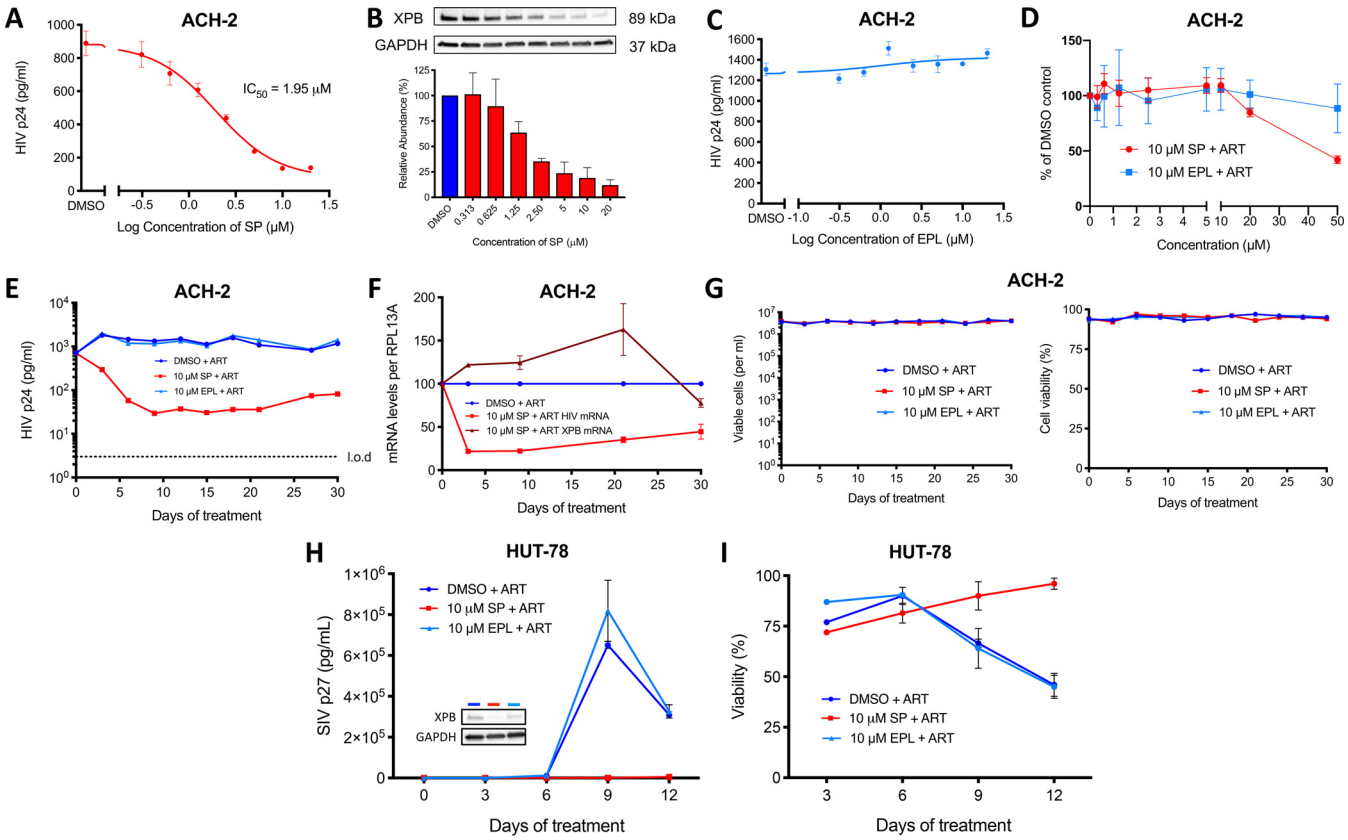

FIG 2 Tat-TAR-independent inhibition of the ACH-2 T cell model of HIV latency and suppression of SIV infection with SP treatment. (A) ACH-2 cells were treated with ART and the indicated concentrations of SP for 72 h, after which the amount of HIV capsid was measured in the supernatant by p24 ELISA. The IC_{50} value was calculated using GraphPad Prism. The line represents the mean of three independent experiments, each with three technical replicates. Error bars represent SD. (B) Cells treated in panel A were collected for Western blotting analysis with the indicated antibodies. Protein abundance was calculated by normalization to GAPDH levels and plotted relative to that of the DMSO control. A representative blot is shown above the quantification of three independent experiments. Error bars represent SD. (C) ACH-2 cells were treated with ART and the indicated concentrations of EPL for 72 h, and the IC_{50} values were calculated as in panel A. (D) Cytotoxicity of SP- (red) and EPL-treated (blue) cells in ACH-2 cells treated for 72 h with increasing concentrations of SP was measured using an MTT assay and plotted as a percentage of the DMSO control. Error bars represent SD from three independent experiments. (E) ACH-2 cells were split and treated every 72 h in the presence of ART with 10 μM SP (red), EPL (light blue), or vehicle only (DMSO, dark blue). HIV capsid production was quantified by p24 ELISA. The dotted black line at 3 pg/ml represents the limit of detection (LOD). This plot is representative of three independent experiments. (F) Cell-associated HIV mRNA levels (red) and *ERCC3* (XPB) mRNA levels (dark red) were measured at multiple time points during the long-term treatments of ACH-2 cells with 10 μM SP in panel E. cDNA was prepared from RNA extracted from cells pellets and qPCR performed with primers in the Nef region. The results were normalized as the number of viral mRNA copies per RPL13A mRNA and plotted relative to the DMSO-treated control (blue, set to 100% for each time point). Error bars represent SD from the qPCR. (G) The number of viable cells per milliliter of culture (left) and percentage viable cells (right), respectively, were measured by trypan blue staining and an automated cell counter every 72 h during the long-term treatments of ACH-2 cells with 10 μM SP, 10 μM EPL, or DMSO only. (H) HUT-78 cells were infected with SIV239 in the presence of 10 μM SP or 10 μM EPL (or vehicle only, DMSO). Capsid production was monitored over time by p27 ELISA. Inset is a representative Western blot of XPB protein expression 12 days postinfection; the housekeeping gene GAPDH is included as a loading control. (I) Viability of the HUT-78 cells in panel H was measured by trypan blue staining using an automated cell counter. Error bars represent SD of two independent experiments.

Potent suppression of simian immunodeficiency virus (SIV) replication with SP but not EPL or DMSO was observed over a period of 12 days (Fig. 2G). This was accompanied by degradation of XPB by SP treatment as measured by Western blotting on day 12 (Fig. 2H, inset panel). A rapid decline in cellular viability, due to cytotoxic effects of virus replication, was observed in DMSO- and EPL-treated cells where virus replication was allowed to proceed, while the viability of cells treated with 10 μM SP was not adversely affected (Fig. 2I). These results suggest that SP may be used in latency studies in nonhuman primates infected with SIV.

In sum, these results suggest that SP inhibits HIV-1 transcription in established cell line models of latency.

RNA silencing of the XPB gene inhibits HIV-1 transcription. To confirm that HIV-1 inhibition by SP was truly dependent on XPB degradation, and not the result of an off-target effect, we knocked down the XPB gene, *ERCC3*, by short hairpin RNA

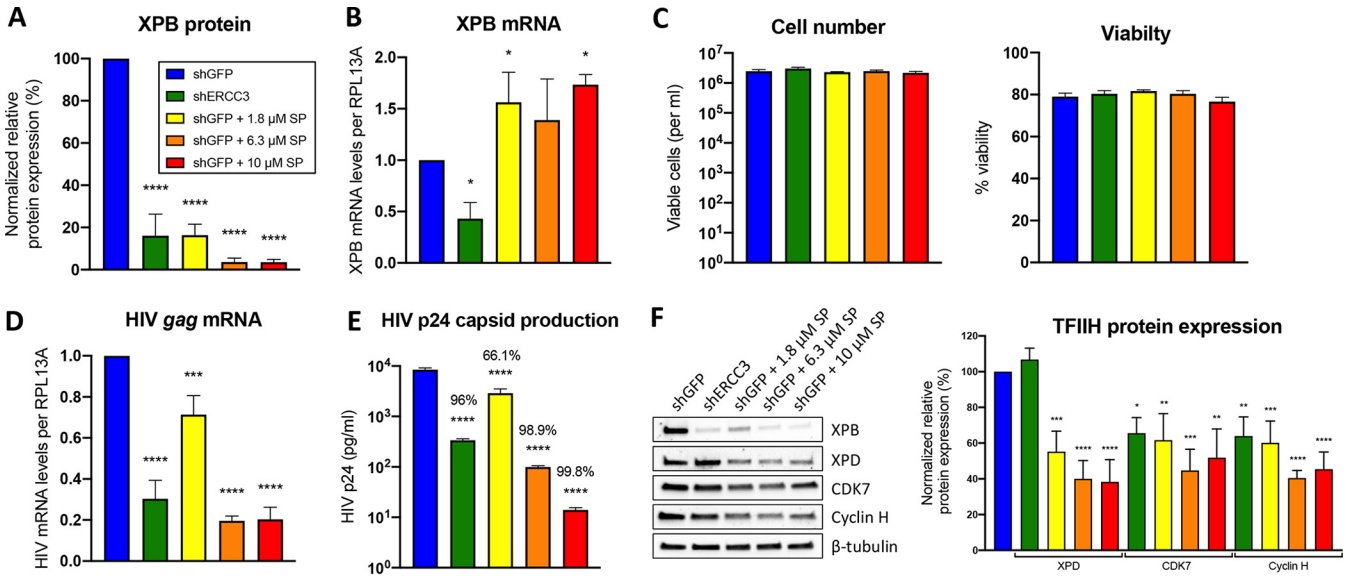

FIG 3 shRNA knockdown of the XPB gene, *ERCC3*, results in similar levels of HIV-1 inhibition in OM-10.1 cells. OM-10.1 cells were transduced with pLKO.1 puro lentiviral vector expressing either a control shRNA targeting *GFP* mRNA or an *ERCC3* (XPB) shRNA. shGFP-transduced cells were also treated with 1.8 μM (IC_{50}), 6.3 μM (IC_{90}), and 10 μM SP. After 10 days of puromycin selection in the presence of ART and DMSO or indicated concentrations of SP, cells were harvested for Western blotting, p24 ELISA, and RT-qPCR analysis. (A) Quantification of the XPB Western blots from three independent experiments. XPB expression was normalized to β-tubulin expression and plotted as a percentage of the shGFP control. (B) *ERCC3* (XPB) mRNA levels were measured by synthesizing cDNA from cell-associated RNA from transduced cells followed by RT-qPCR. Expression was normalized to RPL13A levels and plotted relative to the shGFP control. (C) The number of viable cells (left) and percentage of viable cells (right) were determined using trypan blue staining and an automated hemocytometer. (D) Cell-associated HIV mRNA levels were quantified by RT-qPCR and normalized to RPL13A expression. Levels were plotted relative to the shGFP control. (E) The amount of HIV p24 capsid protein released into the supernatant of transduced OM-10.1 cells were measured by p24 ELISA. (F) In the left panel, a representative Western blot of indicated proteins from 3 independent experiments. The housekeeping gene β-tubulin was included as a loading control. In the right panel, quantification of the XPD, CDK7, and cyclin H Western blots, respectively, from three independent experiments. Protein expression was normalized to the respective housekeeping gene expression and plotted as a percentage relative to the shGFP control. Error bars represent the SD from three independent experiments. *, $P < 0.05$; **, $P < 0.01$; ***, $P < 0.001$; ****, $P < 0.0001$. NS unless indicated. One-way ANOVA followed by the Dunnett multiple-comparison test.

(shRNA) and assessed viral replication. OM-10.1 cells were transduced with a lentiviral vector carrying either an *ERCC3*-specific shRNA or an shRNA targeting the green fluorescent protein (GFP) gene (shGFP) as the control (since these cells do not contain GFP). In parallel, cells transduced with shGFP were treated with an IC_{50} of 1.8 μM and a 90% inhibitory concentration (IC_{90}) of 6.3 μM of SP, as well as 10 μM SP, to compare XPB levels and HIV replication. After 48 h of culture, cells were placed back on ART and selected with puromycin to enrich for cells containing the shRNA. After 10 days of puromycin selection, HIV-1 capsid production in the supernatant was measured by p24 ELISA, and cells were collected for RNA and Western blotting analysis.

Knockdown efficiencies of 60% and 80% at the protein and mRNA levels, respectively (Fig. 3A and B), were achieved with the shRNA targeting *ERCC3* while well tolerated by cells (Fig. 3C). Notably, SP treatment resulted in a slight upregulation of *ERCC3* mRNA (Fig. 3B) as previously observed (Fig. 1F), which we suspect is a cellular compensatory mechanism for the loss of XPB protein. When compared to cells transduced with the shGFP control, the *ERCC3* knockdown resulted in suppression of HIV *gag* mRNA and p24 production to levels between the IC_{50} and IC_{90} concentrations of SP (Fig. 3D and E).

Importantly, when we compared expression of additional TFIIH components, we observed substantial downregulation of XPD, CDK7, and cyclin H with SP treatment (Fig. 3F). With *ERCC3* knockdown, despite XPB downregulation similar to the IC_{50} and IC_{90} concentrations of SP, XPD was not downregulated (Fig. 3F). However, although not to the same degree as SP, loss of CDK7 and cyclin H was still detected (Fig. 3F).

Altogether, our results strongly support that the inhibition of HIV-1 transcription observed with SP treatment is the result of XPB degradation.

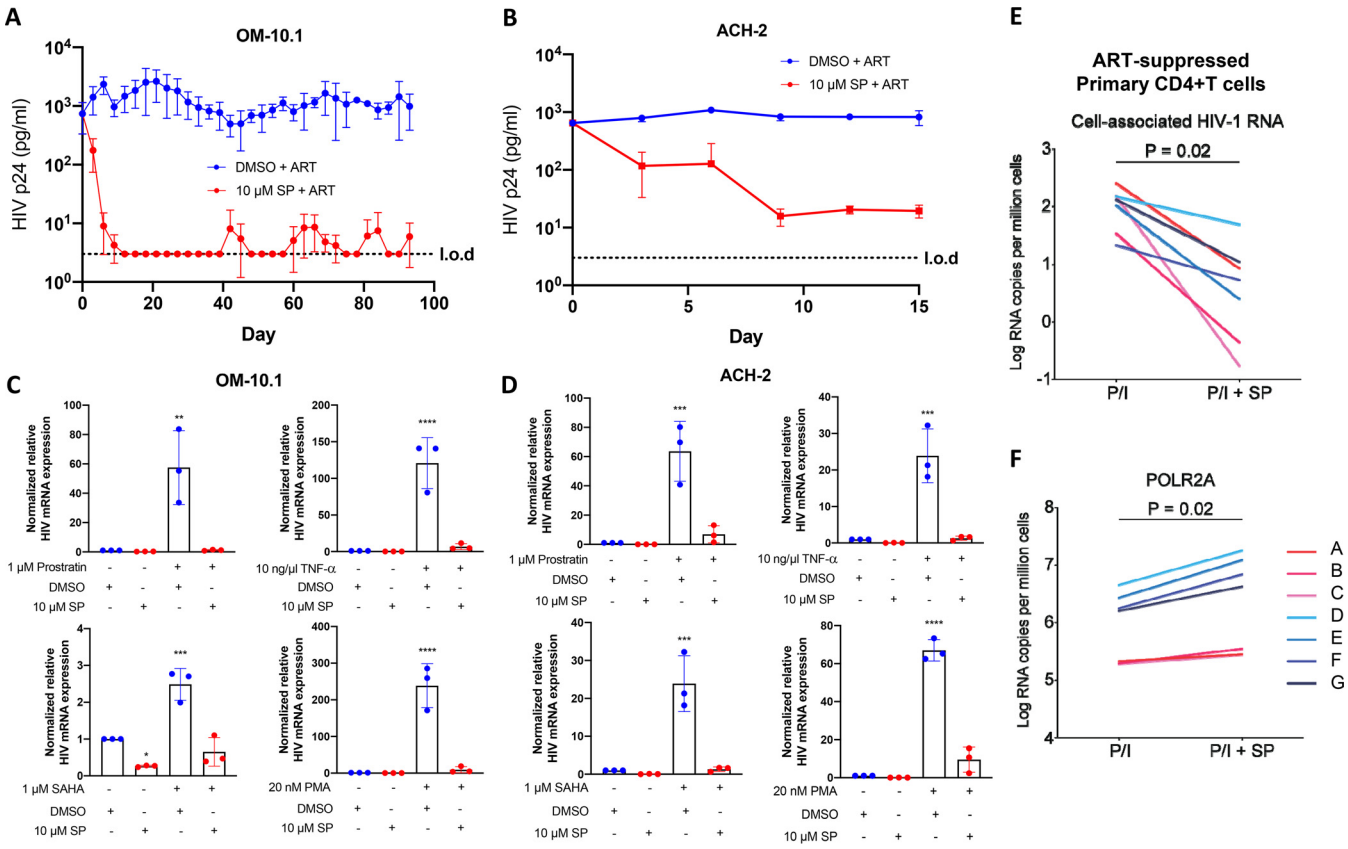

FIG 4 SP treatment blocks HIV reactivation. (A) OM-10.1 cells were treated for 93 days with ART and 10 μM SP or DMSO. Every 3 days, the cells were split, treated, and the amount of p24 capsid released into the supernatant of each culture was measured by p24 ELISA. (B) ACH-2 cells were treated for 15 days with ART plus 10 μM SP or DMSO and treated as for OM-10.1 cells above panel A. (C) After 45 days of treatment, OM-10.1 cells from panel A were set aside from each long-term treatment with ART and 10 μM SP (red) or DMSO (blue) and were stimulated with the indicated concentrations of LRAs for 8 h. The amount of cell-associated HIV mRNA was determined by RT-qPCR, normalized to RPL13A levels, and plotted relative to the unstimulated DMSO control. (D) The same was done on day 15 of long-term ACH-2 treatments with ART and 10 μM SP or DMSO (shown in panel B). (E) Resting CD4$^+$ T cells from 18 ART-treated, virally suppressed individuals living with HIV were isolated from whole PBMCs. Individuals had to have been on ART for >1 year with no "blips" in viral load in the past 6 months. Cells were treated with SP for 24 h in the presence of the fusion inhibitor, T20, to prevent new rounds of infection. In the final 6 h of treatment, cells were subjected to stimulation with PMA + ionomycin. The amount of HIV-1 RNA was measured per million cells. (F) The amount of *POLR2A* mRNA was measured as in panel E. The limit of detection (LOD) is shown by the dotted line at 3.0 pg/ml. Error bars represent the SD from three independent experiments. *, $P < 0.05$; **, $P < 0.01$; ***, $P < 0.001$; ****, $P < 0.0001$. NS unless indicated. A paired *t* test was used to compare stimulated to unstimulated for each respective treatment. A Wilcoxon matched-pairs signed rank test was used to calculate the *P* values for panels E and F.

Treatment of latently infected cells with SP reduces HIV-1 reactivation from latency. We next investigated whether SP treatment could block the reactivation of latent HIV-1 proviruses when cells were exposed to LRAs. The specific LRAs and doses chosen to reactivate each cell model were selected based on the ability to potently stimulate HIV-1 replication with minimal toxicity. Prostratin, phorbol myristate acetate (PMA), and tumor necrosis factor alpha (TNF-α) activate transcription by induction of NF-κB, while the histone deacetylase (HDAC) inhibitor suberoylanilide hydroxamic acid (SAHA) promotes chromatin acetylation, namely, at Nuc-1 on the HIV-1 LTR (60–63).

OM-10.1 and ACH-2 cells were treated for 90 and 15 days, respectively, with 10 μM SP or DMSO, and the levels of HIV-1 capsid production were monitored over time by p24 ELISA (Fig. 4A and B). Cell number and viability remained stable over time (as in Fig. 1 and 2). Once HIV levels had stabilized at maximal inhibition, the cells were treated with a panel of LRAs in the presence of ART and either 10 μM SP or DMSO. After an 8-h incubation period, cells were collected and viral transcription was assessed by reverse transcriptase quantitative PCR (RT-qPCR) to HIV *nef* mRNA. Robust reactivation was observed in DMSO+ART-treated OM-10.1 and ACH-2 cells (Fig. 4C and D, blue bars) with all LRAs tested. While some reactivation of HIV in SP-treated OM-10.1 and

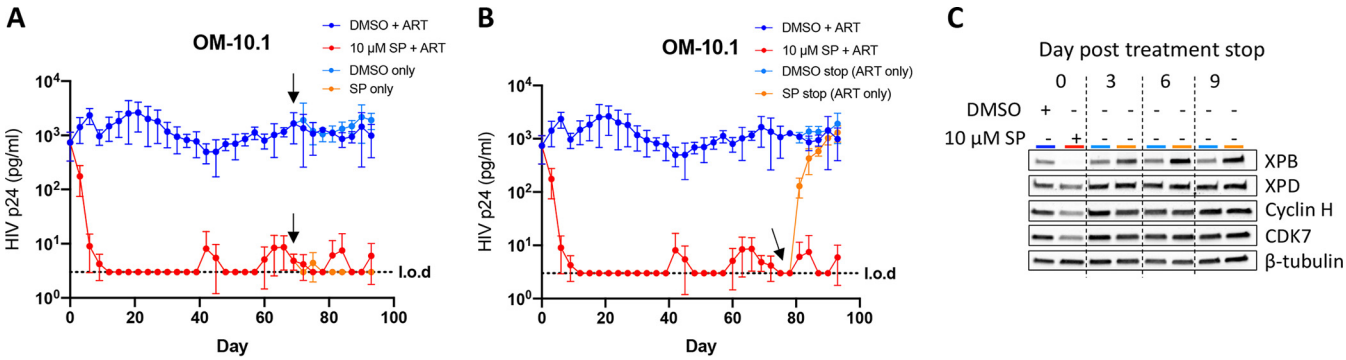

FIG 5 SP treatment of OM-10.1 cells suppresses HIV in the absence of ART, but pretreatment does not delay rebound upon treatment interruption. (A) On day 69 of the long-term treatment of OM-10.1 cells with ART and 10 μM SP or DMSO, some cells were set aside and washed to remove ART (indicated by the black arrows) and maintained alongside the treatments with ART. Cells were then treated every 3 days with DMSO+ART (dark blue), 10 μM SP+ART (red), DMSO with no ART (light blue), or 10 μM SP with no ART (orange). The amount of HIV capsid released into the supernatant was monitored over time by p24 ELISA. (B) On day 78 of the long-term treatment of OM-10.1 cells with ART and 10 μM SP or DMSO, some cells were set aside and washed to remove treatments with DMSO or SP (indicated by the black arrow). Cells were then treated every 3 days with DMSO+ART (dark blue), 10 μM SP+ART (red), ART with no DMSO (light blue), or ART with no SP (orange). The amount of HIV capsid released into the supernatant was monitored over time by p24 ELISA. (C) Cells were collected every 3 days from when DMSO or SP treatments were stopped (light blue and orange lines) for protein expression analysis by Western blotting. A representative blot of the indicated proteins is shown. The limit of detection (LOD) is shown by the dotted line at 3.0 pg/ml. Error bars represent the SD from three independent experiments.

ACH-2 cells was observed in the presence of LRAs, these were non-statistically significant (Fig. 4C and D, red bars). Similar results were observed in the Jurkat latency models (J-Lat A1 and A2) (data not shown).

Next, we assessed the activity of SP in primary cells from ART-adherent individuals living with HIV. Resting CD4$^+$ T cells were isolated from peripheral blood mononuclear cells (PBMCs) from seven individuals with undetectable HIV viral loads, adherent to ART for at least 1 year with no viral load "blips" in the last 6 months. These cells were treated for 24 h with either 10 μM SP or vehicle only in the presence of the entry inhibitor T20, to prevent novel infections. In the final 6 h of treatment, cells were challenged with PMA/ionomycin for T cell activation. SP treatment reduced HIV-1 reactivation an average of 1.4 log (27.6-fold) measured by RT-qPCR per million cells (Fig. 4E). The expression of a housekeeping gene *POLR2A* was also measured and showed modest yet significantly increased levels (an average of 0.4 log; 2.5-fold) (Fig. 4F) (64). These results demonstrate that SP inhibits reactivation from latency in primary CD4$^+$ T cells explanted from virally suppressed individuals.

In sum, these results show that treatment of latently infected cell lines, and *ex vivo* stimulated primary CD4$^+$ T cells, with 10 μM SP dramatically reduces reactivation of HIV-1 from latency when exposed to potent LRAs.

SP treatment alone blocks viral reactivation; however, long-term SP treatment does not prevent viral rebound upon treatment interruption. The long-term treatment of HIV-1-infected cells with the Tat inhibitor dCA results in the accumulation of epigenetic marks at the HIV-1 promoter that render reactivation from latency very difficult to occur upon treatment interruption or stimulation with LRAs (41, 43, 44). Thus, we investigated whether SP treatment over time would lead to similar effects. First, we tested whether 10 μM SP alone was sufficient to maintain HIV transcription suppression in the absence of ART. As such, we washed off ART on day 69 from the OM-10.1 cell culture (three independent experiments) and measured viral p24 production in the supernatant (Fig. 5A, black arrows). A nonsignificant increase in HIV-1 p24 production was observed in DMSO-treated cells in the absence of ART (Fig. 5A, light blue line), while no such increase was observed in SP-treated cells (Fig. 5A, orange line), suggesting that SP treatment alone is able to block HIV replication in the absence of ART. Next, we assessed whether pretreatment with SP would delay HIV rebound upon all treatment interruption; as such, on day 78, DMSO and SP were washed off and cells maintained on ART alone (Fig. 5B, black arrow). As expected, HIV p24 levels remained stable in cells pretreated with DMSO; however, within 12 days, a rapid increase in virus

replication back to DMSO levels was observed in cells pretreated with SP (Fig. 5B, orange line). Concomitantly, within 3 days of treatment interruption, we observed a rapid rebound in XPB protein levels as well as other TFIIH components (XPD, CDK7, and cyclin H) (Fig. 5C). In fact, XPB levels rebounded above the level of the DMSO control and remained elevated for at least 9 days post treatment interruption (Fig. 5C, orange lanes versus light blue lanes).

While pretreatment with SP did not result in long-lasting epigenetic control of viral transcription upon treatment interruption, SP treatment alone seems sufficient to maintain HIV transcriptional inhibition in the absence of ART. These important results suggest that SP blocks HIV transcription as a single therapy and holds great potential to be used in combination with other latency-promoting agents (LPAs), with the goal of establishing an epigenetic lock on the HIV genome.

SP treatment reduces RNAPII recruitment to the HIV-1 genome. To confirm that transcriptional inhibition is the mechanism of action of SP against HIV, we investigated RNAPII recruitment to the HIV-1 genome. As such, we performed chromatin immunoprecipitation (ChIP) to RNAPII followed by qPCR using primers recognizing the HIV-1 genome. We sought to identify differences in occupancy of total as well as phosphorylated Ser5 or Ser2 RNAPII (pSer5, pSer2 RNAPII).

Three independent long-term treatments (~70 days) of OM-10.1 cells with DMSO+ART or SP+ART (Fig. 4A) were treated or not with 1 μM prostratin for 8 h, resulting in a mean 4.3-fold increase in p24 production and a mean 147-fold increase in HIV mRNA (data not shown) in DMSO+ART-treated cells, with no detectable changes in p24 production in SP-treated cells observed (but a mean 5.3-fold increase in HIV mRNA) (data not shown). These cells were cross-linked and prepared for RNAPII ChIP. Without prostratin, with or without SP, a small peak of RNAPII was observed at the HIV promoter (position of ~450 nt) with very little occupancy throughout the genome (Fig. 6A). Modest reductions in occupancy of total pSer5 and pSer2 RNAPII in unstimulated SP+ART-treated cells were observed compared to those of the DMSO+ART control (Fig. 6B and C, red versus dark blue lines). Stimulation with prostratin led to a significant increase of total RNAPII occupancy in DMSO+ART-treated cells, with a peak at the promoter and substantial occupancy throughout the genome (Fig. 6A, light blue line). As expected, a strong peak of pSer5 RNAPII was observed at the HIV promoter in DMSO+ART-treated cells stimulated with prostratin, with a slight reduction in the gene body (Fig. 6B, light blue line). A peak of pSer2 RNAPII was observed at the HIV promoter of DMSO+ART-treated cells stimulated with prostratin, drastically decreasing between nucleotide (nt) positions 1000 and 3500 but increasing again toward the 3′ end between positions 6000 and 9000 (Fig. 6C, light blue line). This is consistent with the role of pSer2 in relief of promoter-proximal pausing (mediated by P-TEFb [65, 66]) and recruitment of splicing and RNA processing machinery (mediated by CDK13/12 [66–69]). A significant reduction of RNAPII occupancy (total, pSer5 and pSer2) was observed on the HIV genome when prostratin reactivation was performed in the presence of SP (Fig. 6A to C, orange lines). This is apparent at the HIV promoter but most noticeable along the gene body. Almost no pSer5 RNAPII is observed along the HIV genome beyond the promoter in SP-treated cells, while total and pSer2 RNAPII is still detected at both the promoter and toward the 3′ end of the genome. Importantly, no significant differences were observed in the occupancy of RNAPII (total, pSer5, pSer2) on the promoter of glyceraldehyde-3-phosphate dehydrogenase (GAPDH) or in the gene body of RPL13A (Fig. 6D to F).

In sum, these results indicate that long-term treatment of cells with 10 μM SP significantly reduces RNAPII occupancy on the HIV genome and potently suppresses RNAPII recruitment upon prostratin stimulation. These effects are not observed on the promoter or open reading frame (ORF) of housekeeping genes.

Long-term effects of SP treatment on the cellular transcription apparatus and cell cycle progression. Previous reports have suggested that short-term treatment of cells with 10 μM SP selectively degrades the XPB subunit of TFIIH, leaving other components mostly unaffected (46, 48). Additionally, in short-term studies using

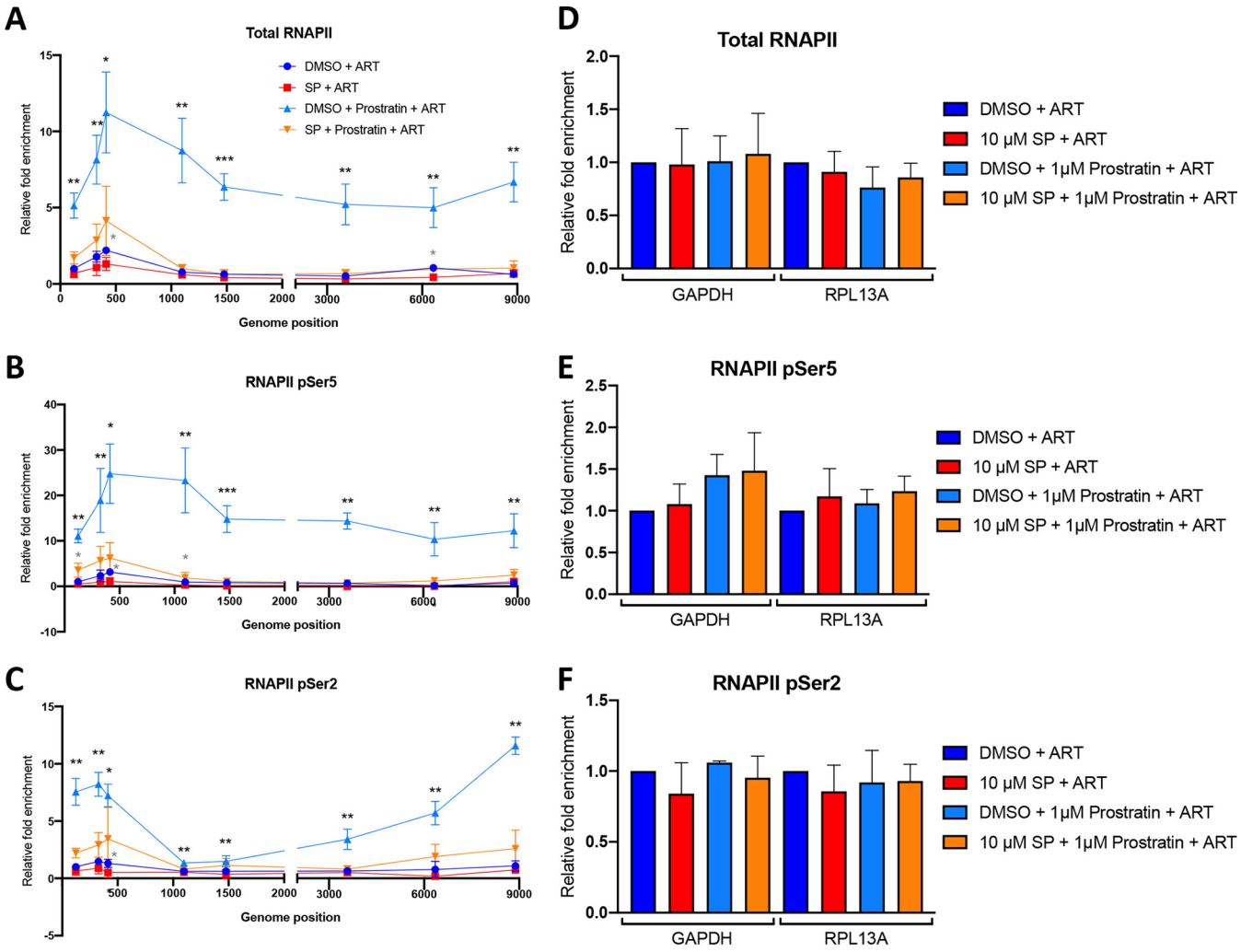

FIG 6 Treatment of OM-10.1 cells leads to a reduction of RNA polymerase II occupancy along the HIV genome. OM-10.1 cells on approximately day 70 from long-term treatments with ART and 10 μM SP or DMSO (Fig. 4A) were set aside and stimulated for 8 h with 1 μM prostratin. Cells were then cross-linked prepared for chromatin immunoprecipitation (ChIP). (A) ChIP to total RNAPII was followed by qPCR with primers specific to the indicated regions on the HIV genome (see Table S2 in the supplemental material). The dark blue and red lines represent the distribution of RNAPII on the HIV genome in unstimulated cells. The light blue and orange lines represent the distribution of RNAPII on the HIV genome when cells were stimulated with 1 μM prostratin for 8 h prior to cross-linking. Data for each point is plotted as a fold enrichment relative to the percentage of input for the unstimulated DMSO control with the first primer set. Gray asterisks mark significance in comparing unstimulated SP-treated cells to unstimulated DMSO-treated cells. Black asterisks mark significance comparing stimulated SP-treated cells to stimulated DMSO-treated cells. (B) As above but using an antibody specific to RNAPII CTD phosphorylated on Ser5. (C) As above but using an antibody specific to RNAPII CTD phosphorylated on Ser2. (D) ChIP to total RNAPII was followed by qPCR with primers specific to the GAPDH promoter region or RPL13A ORF. Data for each point are plotted as fold enrichment relative to the percentage of input for the unstimulated DMSO control with the first primer set. (E) As above but using an antibody specific to RNAPII CTD phosphorylated on Ser5. (F) As above but using an antibody specific to RNAPII CTD phosphorylated on Ser2. *, $P < 0.05$; **, $P < 0.005$; ***, $P < 0.0005$. NS unless indicated. A two-tailed *t* test was performed for the comparison of the different treatment groups in panels A to C. One-way ANOVA followed by the Dunnett multiple-comparison test was used for panels D and E. Error bars represent SD from three independent experiments.

transcriptome sequencing (RNA-seq) and uridine analog 5-ethynyluridine (EU) incorporation assays, Alekseev et al. did not observe global transcriptional defects in SP-treated cells (51). We thus investigated the long-term effects of SP treatment on components of the TFIIH complex as well as on a few important CDKs and respective cyclins. No significant differences were observed in the mRNA expression of any of the TFIIH components in OM-10.1 cells treated with SP for over 100 days (Fig. 7A, cells from Fig. 1E). However, at the protein level, although XPB was by far the most downregulated protein (over 95%), a clear downregulation of other components of TFIIH (namely, XPD, p62, CDK7, and cyclin H) was observed at all time points compared to that for DMSO and EPL (Fig. 7B). In addition, in ACH-2 cells treated for 15 days with 10 μM SP, a similar but more modest reduction in XPD, cyclin H, and CDK7 subunits of

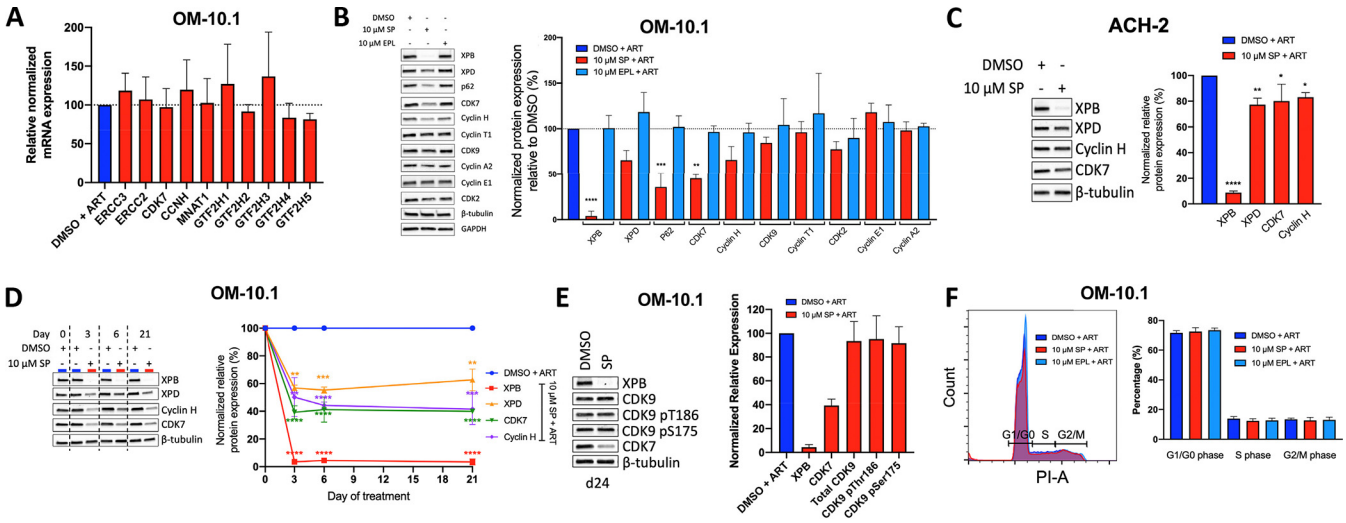

FIG 7 Effects of SP treatment on transcriptional machinery and cell cycle progression. (A) OM-10.1 cells treated for 108, 114, and 123 days with ART and 10 μM SP (red bars) or DMSO (blue bar) (Fig. 1E) were collected for analysis of mRNA expression of the indicated components of TFIIH. cDNA was prepared from cell-associated RNA and qPCR was performed. The results were normalized per RPL13A and plotted relative to the DMSO-treated control (set to 100%, dotted line). Error bars represent the SD from three independent time points. (B) In the left panel, a representative of three independent Western blots of the indicated proteins from OM-10.1 cells treated for 108, 114, and 123 days with ART and DMSO, 10 μM SP, or 10 μM EPL. In the right panel, quantification of the Western blots on the left, protein expression of the indicated genes was normalized to the housekeeping gene, GAPDH, or β-tubulin, and expressed relative to the corresponding DMSO-treated control (set to 100%, dotted line). (C) In the left panel, a representative Western blot of the indicated genes in ACH-2 cells treated for 15 days with ART and 10 μM SP or DMSO only. In the right panel, Western blotting quantification of three independent experiments. The protein expression levels were determined by quantification of the blots, normalized to the housekeeping gene β-tubulin, and expressed relative to the DMSO-treated control (set to 100%, dotted line). (D) In the left panel, a representative Western blot of three independent experiments measuring the protein expression of the indicated genes over time (day 0, day 3, day 6, and day 21). OM-10.1 cells were treated with ART plus 10 μM SP or DMSO for the indicated number of days before harvesting cells for Western blotting. In the right panel, quantification of the Western blots on the left for the indicated proteins, levels were normalized to the housekeeping gene, GAPDH, or β-tubulin, and expressed relative to the corresponding DMSO-treated control (set to 100%). (E) OM-10.1 cells were treated with ART+DMSO or 10 μM SP for 24 days, after which cells were collected for Western blotting analysis of the indicated proteins. In the left panel, a representative Western blot of 3 independent experiments. In the right panel, quantification of the three Western blots, protein expression of the indicated genes was normalized to the housekeeping gene, GAPDH, or β-tubulin, and expressed relative to the corresponding DMSO-treated control (set to 100%). (F) OM-10.1 cells were treated with ART and either DMSO, 10 μM SP, or 10 μM EPL for ~80 days. Cell cycle stage analysis was performed by propidium iodide staining and flow cytometry 72 h posttreatment. In the left panel, a representative plot showing the degree of PI staining under each treatment condition. In the right panel, a summary of the percentage of cells in the indicated stage of the cell cycle. Error bars represent the SD from three independent experiments. *, $P < 0.05$; **, $P < 0.01$; ***, $P < 0.001$; ****, $P < 0.0001$. NS unless indicated. One-way ANOVA followed by the Dunnett multiple-comparison test.

TFIIH was also observed (Fig. 7C). This downregulation of TFIIH components was detected as early as 72 h after treatment of OM-10.1 cells with 10 μM SP and did not appear to magnify over time (Fig. 7D).

We also investigated whether long-term SP treatment affected the expression and function of other critical CDKs and their cyclin partners, such as P-TEFb (CDK9 and cyclin T1) and cell cycle proteins CDK2, cyclin E1, and cyclin A. No significant differences were observed between SP-, vehicle-, or EPL-treated OM-10.1 cells (Fig. 7B). Recently, CDK7 was shown to be the primary kinase responsible for CDK9 Ser175 phosphorylation thought to bias CDK9's binding from BRD4 to Tat (30). Additionally, it was proposed that CDK7 phosphorylates CDK9 at Thr186, which is required for CDK9 activity, though CDK9 also autophosphorylates at this residue (30, 70). Given SP reduction of CDK7 protein expression (Fig. 7B and D), we compared the levels of pThr186 and pSer175 CDK9 by Western blotting in SP- and vehicle-treated OM-10.1 cells treated for 24 days (Fig. 7E). While potent depletion of XPB and approximately 60% reduction in CDK7 was observed, the levels of total, pThr186, and pSer175 CDK9 remained unchanged. Furthermore, by propidium iodide (PI) staining, no differences in cell cycle progression between treatment groups were observed (Fig. 7F).

In sum, although long-term treatment of cells with 10 μM SP results in a reduction in protein levels of additional components of the TFIIH complex besides XPB, we did not observe differences in the expression of other important kinases, cyclins, housekeeping genes, phosphorylation of CDK9, or in cell cycle progression.

Treatment of latently infected cells with SP reduces HIV-1 transcription without global dysregulation of cellular mRNA expression. Due to the critical nature of TFIIH for RNAPII-mediated transcription and the significant loss of some of the components of TFIIH in addition to XPB (Fig. 3F, 5C, and 7), we investigated global cellular mRNA synthesis defects that may occur with SP treatment. As such, we treated OM-10.1 cells for 15 days with either SP+ART or DMSO+ART (once maximal HIV inhibition had been achieved in the SP-treated cells), followed by RNA extraction and mRNA-seq analysis. For this study, we included cells stimulated or not with the protein kinase C (PKC) agonist prostratin to assess effects on activation-dependent genes. HIV encoding genes were among the most significantly downregulated genes in cells treated with SP compared to those of the DMSO control, particularly upon stimulation with prostratin (Fig. 8A, left and right, red points). Some of the most significantly affected cellular genes are highlighted and labeled in blue [pAdj $<$ 1e$-$10 and abs(log2-fold change) $>$ 1 for SP versus DMSO comparisons (Fig. 8A, left and right; see also Tables S1 and S2 in the supplemental material) and pAdj $<$ 1e$-$30 with an abs(log2- fold change) $>$ 2.5 for stim versus no stim comparisons (Fig. 8A, middle two panels; see also Tables S3 and S4 in the supplemental material)]. In unstimulated cells, treatment with SP resulted in the upregulation of 49 genes and downregulation of 25 compared to those of the DMSO control [Fig. 8A left panel; pAdj $\leq$ 0.05, log2 FC $\geq$ abs(1)]. Prostratin stimulation led to the differential expression of 758 genes in DMSO-treated cells and 823 genes in SP-treated cells (546 of which were differentially expressed between conditions) (Fig. 8A, middle panels). SP treatment, while specifically affecting the expression of some genes, does not appear to affect all RNAPII-mediated transcription, which is in support of previous studies suggesting XPB depletion by SP does not affect global cellular transcription (51). To determine more rigorously what patterns of gene signaling pathways were affected by SP treatment, we performed gene set enrichment analysis (GSEA) (71). A bubble-lattice plot was constructed to highlight gene sets affected by SP treatment, where the color of the bubble represents the normalized enrichment score (NES) (indicating the number and differential intensity of the assessed genes in each indicated pathway), and statistical significance is indicated by the size of the bubble (Fig. 8B). HIV-encoded genes were significantly downregulated compared to DMSO control, particularly under conditions of prostratin stimulation, indicating the strong specific effect of SP treatment on HIV transcription (Fig. 8B). Of note, with this type of bubble representation of the data, it is important to keep in mind the size of the gene set; for instance, the MYC targets have modest downregulation with SP treatment, but since there are 200 genes in this set, the NES score is of greater magnitude. Conversely, downregulation of HIV genes is greater, but because there are a lot fewer genes in this set, the NES is of lower magnitude. Genes related to DNA packaging (histone- and chromatin-related genes) were significantly upregulated in both unstimulated and prostratin stimulated SP-treated cells (Fig. 8B). Conversely, MYC targets, E2F targets, RNAPII transcription termination, and type I interferon (IFN-I) receptor binding genes were downregulated with SP treatment, which increased in significance upon prostratin stimulation (Fig. 8B). Furthermore, cellular (endogenous) genes involved in the late phases of the HIV life cycle (reactome gene sets [72]) were modestly downregulated upon stimulation, which include genes involved in transcription, RNA processing, and export from the nucleus (Fig. 8B). IFN-γ response genes were slightly upregulated in unstimulated SP-treated cells, gaining significance upon stimulation (Fig. 8B). Other gene sets related to transcription of the HIV genome, RNAPII elongation, IFN-α response, housekeeping, and apoptosis were not substantially affected (Fig. 8B). Heatmaps were constructed from transcripts per million (TPM) data to facilitate direct comparison of gene expression with different lengths (Fig. 8C; see also Table S5 in the supplemental material). All HIV genes were clearly downregulated upon SP treatment and, although prostratin stimulation increased HIV expression, this was substantially reduced compared to that of DMSO-treated cells (Fig. 8C, left). Because of the modest downregulation in genes involved in the late phase of the HIV life cycle observed in the GSEA (Fig. 8B), we examined the expression of individual genes within this set.

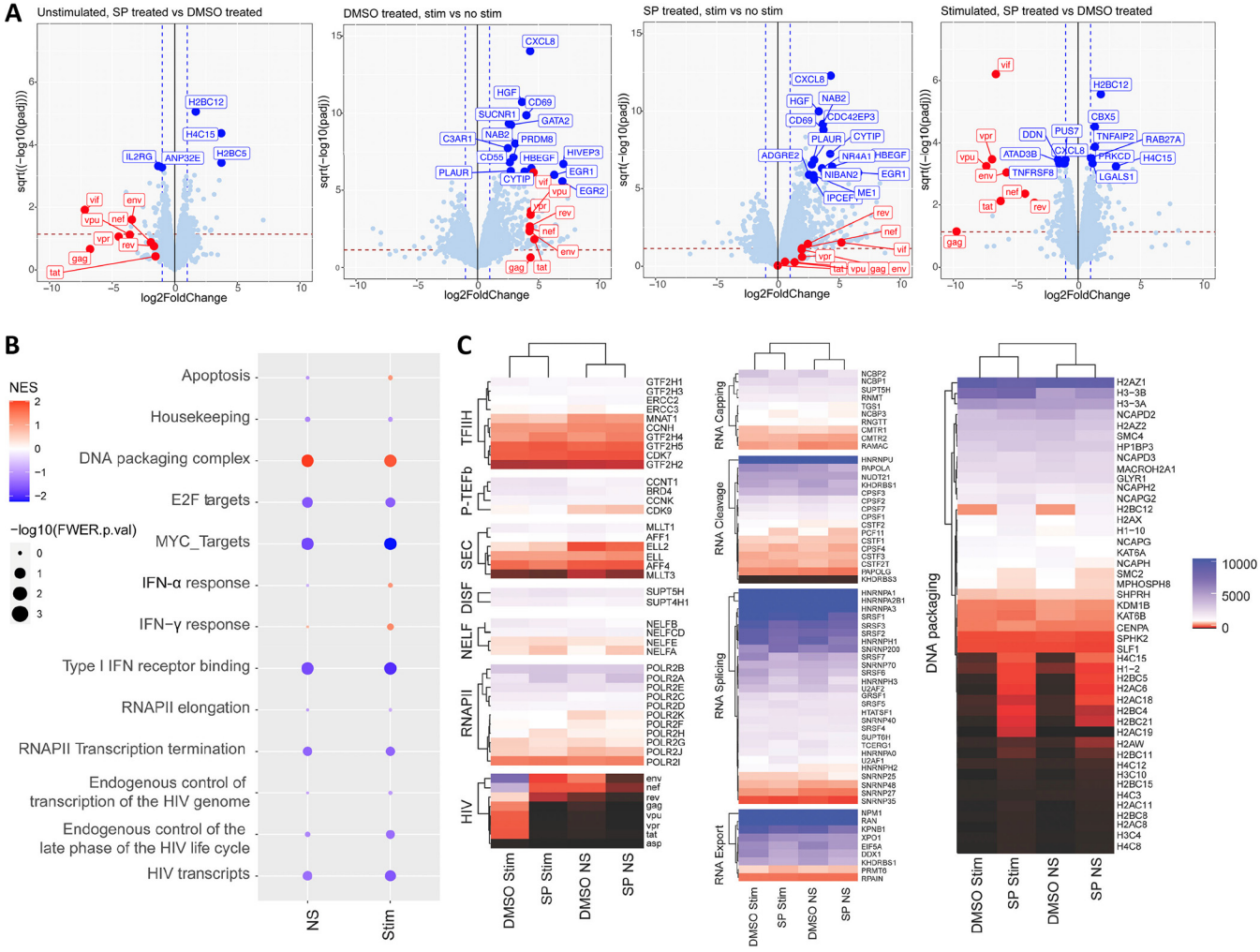

FIG 8 Potent inhibition of HIV mRNA expression with limited effects on cellular transcription. OM-10.1 cells were treated with ART+DMSO or ART plus 10 μM SP for 15 days (until HIV capsid production in supernatant in SP-treated cells stabilized to below the limit of detection by p24 ELISA) followed by an 8-h stimulation (or not) with 1 μM prostratin. mRNA-seq and differential expression analysis were performed on these cells. Data are from two biological replicates. (A) Volcano plots showing differentially expressed genes under the indicated conditions. HIV encoding genes are colored red and the most significantly differentially expressed genes are colored blue [pAdj < 1e-10 & abs(log2 fold change) > 1 for SP versus DMSO comparisons (left and right) and padj < 1e-30 with an abs(log2 fold change) > 2.5 for stim versus no stim comparisons (middle two panels)]. The horizontal dotted line represents a pAdj = 0.05 and the vertical dotted lines a log2 FC of 1 and −1. In the left panel, the change in expression of all genes (dots) in SP-treated compared to DMSO-treated cells without stimulation. In the middle left panel, differentially expressed genes in DMSO-treated cells stimulated with prostratin compared to those of unstimulated cells. In the middle right panel, differentially expressed genes in SP-treated cells stimulated with prostratin compared to those of unstimulated cells. In the right panel, differentially expressed genes in prostratin-stimulated cells treated with SP compared to DMSO. (B) GSEA bubble-lattice plot of selected gene sets. The color represents the normalized enrichment score (NES) indicating the number and differential intensity of the assessed genes in each indicated pathway. NES > 0, the gene set is enriched in the SP-treated sample (red). NES < 0, the gene set is enriched in the DMSO-treated sample (blue). NS, unstimulated; Stim, prostratin stimulated. The size of the dots indicates the statistical significance of the enrichment found (log transformed familywise error rate, $-\log_{10}$ FWER *P* value). GSEAs were computed from the GSEA app version 4.1.0 using TPMs as counts and publicly available gene sets current as of October 2020 (71). (C) Heat map of expression levels (transcript per kilobase million [TPM] values) for selected genes with DMSO or SP treatment, with and without stimulation with prostratin.

Expression of transcription-related genes, such as TFIIH, P-TEFb, the SEC, NELF, DSIF, and RNAPII genes do not appear to be substantially affected by SP treatment (Fig. 8D, left). Furthermore, there were no obvious differences in expression of RNA splicing, export, capping, or cleavage genes between SP- and DMSO-treated cells (Fig. 8C, middle). These results are consistent with previous results, in which SP did not affect the transcriptional machinery and cell cycle progression (Fig. 7) but blocked HIV reactivation (Fig. 4). Nonetheless, SP treatment does curiously seem to upregulate a large subset of DNA packaging complex genes (Fig. 8C, right panel), which is often associated with defects in cell cycle progression (73). However, this upregulation might not be biologically significant since, as mentioned above, no obvious differences in cell division were observed in SP-treated cells (Fig. 7).

In sum, SP treatment results in robust suppression of HIV transcripts both in unstimulated or prostratin stimulated cells, consistent with the observations in Fig. 1 and 4. While the expression of a few specific gene sets was significantly impacted by SP treatment, we hypothesize that their fold change may not be biologically significant since no major defects were observed in cell growth and viability. Nevertheless, the effects of SP treatment at concentrations sufficient to potently degrade XPB will need to be assessed *in vivo*.

DISCUSSION

Inhibiting transcription from latent proviruses is an increasingly attractive approach for a functional cure for HIV-1. The long-term transcriptional inhibition of HIV-1 may lead to a sustained epigenetic repression with the potential to contain viral transcription even in the absence of ART (43, 44). In addition, such transcriptional inhibition may reduce "blips" or moments of detectable viremia observed in some virally suppressed patients as well as chronic immune activation that stems from the continuing trickling of HIV transcription and viral protein production observed under suppressive ART. To date, there are unfortunately no FDA-approved HIV-1 transcriptional inhibitors available. In this study, we investigated the potential of the clinically approved drug SP, which targets the host transcription factor XPB for proteasomal degradation, for the inhibition of latent HIV-1 in various cell line models and primary $CD4^+$ T cells from virally suppressed individuals.

In agreement with previous studies, we observed a dose-dependent reduction of XPB protein levels with SP treatment (Fig. 1B and 2B) (46–48, 51), which parallels a dose-dependent reduction in HIV-1 replication (Fig. 1A and 2A). Here, we showed that specific shRNA knockdown of XPB resulted in similar HIV inhibition, suggesting that HIV inhibition by SP treatment is specifically mediated by XPB protein levels (Fig. 3). Importantly, EPL, a more specific MR antagonist, does not inhibit HIV or degrade XPB (Fig. 1C and 2C). Thus, HIV inhibition by SP is independent of MR antagonism and dependent on the degradation of the host helicase XPB. Contrary to previous reports that showed short-term SP treatments selectively degrade XPB, leaving other subunits of TFIIH relatively intact (47, 48, 51), we show that even after a short 72-h period, the levels of XPD, p62, CDK7, and cyclin H but not other cellular proteins were significantly reduced (Fig. 3F, 5C, and 7). These effects seem to be somewhat cell type specific since they were more pronounced in OM-10.1 than in ACH-2 cells (Fig. 7B versus Fig. 7C). This could be explained either by more modest XPB degradation in ACH-2 cells (Fig. 1B versus Fig. 2B), or it could be related to the absence of a functional Tat-TAR feedback loop in ACH-2 cells. This warrants further investigation. It remains to be determined whether loss of other TFIIH subunits is due to destabilization of the complex or to off-target proteasomal degradation. Of note, shRNA knockdown of the XPB gene, *ERCC3*, does not result in the same degree of TFIIH components loss (Fig. 3F). While reduction of XPB with *ERCC3* shRNA knockdown was around that observed with 1.8 μM SP treatment, we do not observe any loss of XPD and a more modest loss of CDK7 and cyclin H. Importantly, *ERCC3* knockdown showed no cytotoxic or cytostatic effects (Fig. 3C). Although shRNA knockdown of XPB resulted in an ~80% reduction of XPB protein (similar to treatment with 1.8 μM SP) (Fig. 3A) with less effects on other TFIIH components, it reduced HIV mRNA levels to a greater degree than 1.8 μM SP treatment, further suggesting that development of more specific XPB degraders may improve on SP potency and could potentially avoid unwanted off-target transcriptional activity as well as the other known effects of SP on the MR.

Treatment of latently infected cells with SP results in a rapid, robust suppression of HIV transcription, and reactivation using LRAs is significantly inhibited (Fig. 4). Importantly, SP treatment blocks the strong HIV-1 reactivation by PMA/ionomycin in $CD4^+$ T cells explanted from ART-suppressed individuals living with HIV (Fig. 4E). While levels of HIV reactivation were substantially reduced with SP treatment (average of 27.6-fold), the levels of the housekeeping gene *POLR2A* (encoding a subunit of RNAPII)

were modestly elevated (average of 2.5-fold) (Fig. 4F). The slight increase in *POLR2A* observed in primary cells upon SP treatment requires further investigation to determine whether this is a direct consequence of SP activity or is related to inhibition of HIV transcription. Of note, even if not statistically significant ($P = 0.78$), the mRNA-seq analysis in OM-10.1 cells showed a slight increase in *POLR2A* expression in cells treated with SP stimulated with prostratin compared to that of DMSO (log2 FC of 0.5). Furthermore, there were no obvious changes in expression of other RNAPII subunits (Fig. 8D, middle).

Importantly, SP treatment was shown to be sufficient to maintain HIV p24 production below the limit of detection in the absence of ART (Fig. 5A). These results highlight the potential of using SP as a single drug to maintain HIV-1 suppression, once deep latency has been established, in the absence of ART. However, regardless of treatment duration in the latent models tested, transcription remains detectable, and once SP treatment is interrupted, there is rapid transcriptional rebound to control levels (Fig. 5B). This was not observed with treatment with dCA, where longer treatment periods led to undetectable levels of viral RNA and sustained viral inhibition when treatment was interrupted (41, 43). The reasons for this difference may be 2-fold. On one hand, since a host component of a transcription factor complex is involved, as soon as XPB is produced again above a certain threshold, it can participate and jumpstart transcription from the viral promoter. In fact, the levels of XPB protein become elevated, and remain so for at least 9 days, upon removal of SP (Fig. 5C), possibly due to elevated XPB mRNA levels with SP treatment (Fig. 1F). On the other hand, since transcriptional inhibition is not fully complete, the residual level of transcription may preclude epigenetic repressive mark deposition for complete silencing of the promoter locus. Future studies will address the benefits of combining SP treatment with other transcriptional inhibitors, such as dCA.

The RNAPII CTD tail contains 52 repeats of the heptad $Y_1S_2P_3T_4S_5P_6S_7$ that serves as a hot spot for posttranslational modification to fine-tune transcription (66, 74–76). Hypophosphorylated RNAPII is recruited to the promoter and is primed for activation by phosphorylation of Ser7 by the CDK7 subunit of TFIIH. Additional phosphorylation of Ser5 by CDK7 activates RNAPII to initiate transcription and escape the promoter; as such, pSer5 levels are highest at the TSS but decrease toward the end of genes. Promoter-proximal pausing of RNAPII occurs due to repressive factors (DSIF and NELF) and occlusion by Nuc-1. RNAPII pausing is relieved through CDK9 phosphorylation of DSIF, NELF, and Ser2 of RNAPII CTD, resulting in a pSer2 peak just downstream of the TSS. Further phosphorylation of Ser2 occurs as RNAPII moves along the gene body, mediated by CDK12/13, resulting in increasing pSer2 levels toward the 3′ end of genes in the gene body and is associated with recruitment of RNA processing and splicing factors (67, 68, 77, 78). Spironolactone treatment results in a loss of RNAPII (total, pSer5, and pSer2) occupancy throughout the HIV genome, particularly noticeable upon LRA stimulation (Fig. 6A to C). In unstimulated cells, little RNAPII is recruited to the promoter of either SP- or DMSO-treated cells, given the low basal HIV expression in these cells. Upon reactivation with prostratin, some RNAPII was still detected at the TSS in SP-treated cells, even with the robust loss of XPB. This is not unexpected since RNAPII is brought to the promoter during PIC formation prior to TFIIH recruitment (14, 15, 17). However, since HIV transcription depends on the positive feedback loop driven by Tat, a reduction in elongation would result in a loss in recycling of RNAPII and reduced overall RNAPII occupancy at the promoter. RNAPII was barely observed in SP+ART-treated cells downstream from the promoter compared to robust recruitment in DMSO+ART-treated cells upon transcriptional reactivation. This is consistent with the role of TFIIH in initiation and promoter clearance (16, 18, 19). Significantly, changes in RNAPII occupancy (total, pSer5, and pSer2 CTD) were not observed at either the promoter of GAPDH or the ORF of RPL13A (Fig. 6D to F), suggesting that the HIV-1 genome is especially sensitive to perturbation of TFIIH and the reduction in RNAPII recruitment is specific to the HIV-1 genome. This is consistent with our own results

(Fig. 8) and previous work, which revealed that genes highly dependent on NF-κB experience reduced RNAPII recruitment with SP treatment while other more constitutively expressed genes were not affected (47). NF-κB has been shown to recruit TFIIH to the inactive RNAPII poised at the HIV TSS to allow CDK7 phosphorylation of RNAPII CTD (53).

TFIIH is a critical general transcription factor involved in the initiation of transcription of most RNAPII-dependent genes, including HIV (14, 15, 19, 53, 79). However, XPB has been proposed to be dispensable for RNAPII-mediated transcription (51). Despite SP treatment mediating substantial XPB degradation and moderate loss of other TFIIH components, SP seems well tolerated by cells treated long-term (Fig. 1G, 2G, and 3C). In addition, SP does not appear to interfere with cell cycle progression, it does not cause significant losses of P-TEFb or cell cycle proteins, and it has no effect on phosphorylation of CDK9 (Fig. 7). In agreement, our mRNA-seq analysis suggests that SP treatment specifically and potently inhibits HIV expression, while more modestly affecting a subset of cellular genes (Fig. 8). We cannot exclude the possibility that HIV transcription is inhibited indirectly through SP-mediated effects on cellular proteins, since GSEA revealed modest reduction in genes involved in the late phase of the HIV life cycle (Fig. 8B). However, SP did not cause obvious changes in mRNA expression (TPM count data) of RNA processing genes (capping, cleavage, splicing, or export) or RNAPII-related transcription factors (TFIIH, P-TEFb, super-elongation complex, NELF, or DSIF) that could have potentially explained the potent downregulation of HIV mRNA expression (Fig. 8C). Intriguingly, histone- and chromatin-related genes (DNA packaging) were among the most upregulated genes upon SP treatment (Fig. 8B and C). However, these changes are probably not significant, since no changes in cell cycle progression were observed (Fig. 7).

Despite an ~95% reduction in XPB levels and between 20 and 60% reduction in some other components of TFIIH with 10 μM SP treatment (Fig. 7), we hypothesize that there are sufficient amounts of this complex to support basal transcription. Activation-dependent genes, such as cytokines and HIV, which require recruitment of large amounts of TFIIH may be more susceptible to XPB loss (47). These results are not unexpected and are consistent with previous reports showing SP treatment does not globally reduce transcription but rather more selectively inhibits HIV and NF-κB-dependent transcription (47, 48, 51). Interestingly, mRNA-seq differential expression analysis revealed significant downregulation of *MYC* and MYC-target genes (Fig. 8B). This is consistent with the known role of XPB regulating c-*MYC* expression through far upstream sequence element (FUSE) binding protein (FBP) and the FBP-interacting repressor (FIR), which bind to the FUSE (80, 81). FBP/FIR act in response to cellular signals to control RNAPII pausing and release through interactions with the XPB subunit of TFIIH to regulate *MYC* expression (82, 83). It is proposed that FBP and FIR binding to TFIIH regulates activation-dependent but not basal *MYC* expression (82). The level of TFIIH in cells is tightly regulated and correlates with transcriptional activity (84). Thus, we expect that inducible genes that become transcriptionally very active upon stimulation may be more susceptible to XPB degradation than those transcribed at a far lower rate.

Further studies are needed to determine the full extent by which SP treatment inhibits HIV transcription, directly via XPB degradation or indirectly via other altered cellular genes, and the mechanisms behind the increased susceptibility of HIV to SP treatment compared to the majority of cellular genes (51).

Although SP has been a very useful tool to tease out the role of XPB in transcription, it will take some additional monitoring for it to be explored for block-and-lock approaches in the clinic. The concentrations of SP needed for maximal XPB degradation and HIV-1 inhibition (10 μM) is well above the peak serum concentrations reached in healthy volunteers administered 100 mg SP daily for 15 days of around 0.19 μM. The area under the curve (AUC) at day 15, reflecting the actual body exposure to the drug was 0.55 μM, which would result in suboptimal XPB degradation (Fig. 1B and 2B) (85).

However, SP is used to treat women experiencing hair loss at 200 mg daily without negative effects, and transgender women take up to 400 mg daily presurgery (86, 87). Additionally, the FDA has approved a 4-week treatment of 400 mg daily SP to diagnose hyperaldosteronism (88). The most common side effects reported at high doses of SP are gynecomastia and the more serious hyperkalemia, which requires monitoring (89). XPB is also involved in nucleotide excision repair and has been proposed as a means to sensitize cells to platinum-based cancer therapies (46). The FDA noted that rats treated with 500 mg/kg/day (about 25 times the human recommended daily dose of 200 mg per day) had an increase in occurrence of benign tumors. The risk of treating individuals with a dose of SP high enough to degrade XPB would need to be assessed, and whether or not these side effects will be a major drawback for clinical testing remains to be seen. SP has, however, great potential to be used in combination with other therapies given its very quick effects on HIV. One could foresee the initial use of high doses of SP to reduce HIV-1 transcription to or below the level of detection, at which point SP doses could be reduced and another inhibitor, such as a Tat inhibitor, could be introduced to bring about a state of "deep latency" from which rebound would be very difficult to occur. Future studies will investigate this combination therapy. Furthermore, combination treatments may allow the use of reduced dosages.

Altogether, we showed here that targeting a host component of a transcription factor complex, XPB, reduces HIV-1 transcription and reactivation from latency without obvious adverse effects on cellular transcription. We show that SP acts additively with ART to reduce HIV-1 transcription and block reactivation from latency upon stimulation with LRAs. Even given some concerns with the high doses of SP required for XPB degradation *in vivo*, our results warrant the exploration of SP as a therapeutic in "block-and-block" approaches for a functional cure.

MATERIALS AND METHODS

Cell lines and cell culture. OM-10.1 and ACH-2 cells were obtained through the NIH AIDS Reagent Program (from S. Butera, no. 1319, and T. Folks, no. 349, respectively). Cells were maintained in RPMI 1640 (Gibco) supplemented with 2.0 mM L-glutamine/100 U/ml penicillin/100 μg/ml streptomycin (Gibco) and 10% heat-inactivated fetal bovine serum (FBS) (Atlas Biologicals; catalog no. FS-0500-AD) (complete RPMI) and cultured at 37°C and 5% CO_2. Cells were passaged every 3 days, and medium was replaced with the indicated concentrations of SP, EPL, or DMSO and an ART cocktail (200 nM lamivudine [AIDS reagent], 200 nM raltegravir [Selleck Chemicals; MK-0518], 100 nM efavirenz [AIDS reagent]). SP was purchased from Sigma-Aldrich (no. 1619006) and dissolved in DMSO (Fisher Scientific; no. BP231-100). EPL was purchased from Sigma-Aldrich (no. E6657-10MG) and dissolved in DMSO. Cell concentration and viability was measured using the TC20 automated cell counter (Bio-Rad; no. 1450102) and trypan blue staining.

Infection of Hut78 cells with SIVmac239. Hut78 cells were infected as previously described (90). Briefly, cells were infected overnight with SIVmac239. Cells were then washed with phosphate-buffered saline, split into 3 flasks, and treated with DMSO, EPL, or SP (10 μM) for 12 days. SIV replication was assessed every 3 days postinfection by measuring the viral capsid in the supernatant with p27 ELISA (Advances Bioscience Laboratories; no. 5436).

Determination of SP half-life in cell culture. Stability of SP was evaluated in cell culture using an AB Sciex 5500 mass spectrometer run in multiple reaction monitoring mode. Cells were treated with 10 μM SP (with or without ART), and the concentration of SP was evaluated before and after 72 h of incubation at multiple time points. Cells were resuspended and treated with 2× vol/vol acetonitrile to lyse the cells, precipitate cellular protein, and inactivate the virus. Samples were filtered through a 0.2-μm filter plate prior to injection onto the LC-MS/MS. LC conditions used a Thermo BetaSil C_{18} 5-μm, 50- by 2.1-mm column with a linear gradient of water + 0.1% formic acid (A) and acetonitrile with 0.1% formic acid (B) (10% B from 0 to 0.5 min, 90% B at 2 to 3 min, 10% B at 4 to 6 min). Detection of SP used the mass transition of 417.3→341. Half-life was calculated by plotting the natural log of the percent remaining compound verses time where $t_{1/2} = \ln(2)/\text{slope}$ of the linear regression.

p24 ELISA. The amount of HIV p24 capsid protein produced in the supernatant of cultured cells was quantified using the antigen capture assay kit from Advanced BioScience Laboratories, Inc. (no. 5447) and performed according to the manufacturer's protocol.

MTT cell proliferation assay. The viability and proliferation of cells treated with increasing concentrations of SP and EPL were measured using the 3-(4,5-dimethylthiazol-2-yl)-2,5-diphenyltetrazolium bromide (MTT) assay according to the manufacturer's protocol (ATCC; no. 30-1010K). Cells were cultured in 96-well plates (in triplicate per drug concentration) for 72 h prior to addition of the MTT reagent.

Western blotting for OM-10.1, ACH-2, and HUT-78 cells. Cells were collected, washed, and lysed with a 20 mM HEPES (pH 8.0), 100 mM KCl, 0.2 mM EDTA, 5 mM β-mercaptoethanol, 0.1% IGEPAL CA-630, 10% glycerol, and supplemented with complete EDTA-free protease inhibitor cocktail (Roche; no.

4693132001) on ice for 10 min. For pSer175 and pThr186 CDK9 Western blotting, we added phosphatase inhibitor cocktail 3 (Sigma-Aldrich; no. P0044-1ML). Protein concentration was determined using the Bio-Rad protein assay dye (no. 50000006). Equal amounts of total protein extract were loaded, alongside the Precision Plus Protein all blue protein standards (Bio-Rad; no. 1610373) onto a precast 4% to 20% gradient stain-free protein gel (Bio-Rad; no. 4568094). Proteins were then transferred to a nitrocellulose membrane using the Bio-Rad Trans-Blot Turbo system (no. 1704270). Membranes were blocked with 5% milk and probed with the following antibodies: anti-XPB (Sigma-Aldrich; no. X0879, diluted 1:2,000), anti-XPD (Cell Signaling Technology; no. 11963S, diluted 1:1,000), anti-CDK7 (Santa Cruz; sc-7344, diluted 1:500), cyclin H (Cell Signaling Technology; no. 2927S, diluted 1:1,000), p62 (Santa Cruz; sc-25329, diluted 1:500), cyclin A2 (Cell Signaling Technology; no. 4656S, diluted 1:1,000), cyclin E1 (Cell Signaling Technology; no. 4129S, diluted 1:500), CDK2 (Cell Signaling Technology; no. 25465S, diluted 1:1,000), CDK9 (Cell Signaling Technology; no. 2316S, diluted 1:1,000), pThr186-CDK9 (Cell Signaling Technology; no. 2549S), pSer175-CDK9 (kind gift from Jonathan Karn), β-tubulin (Proteintech; no. 66240-1-IG, diluted 1:10,000), and GAPDH (Santa Cruz; sc-32233, diluted 1:1,000) in 3% bovine serum albumin (BSA) (or 5% milk for the β-tubulin antibody). Secondary antibodies were anti-mouse (GE Healthcare; no. NA931-1ML) diluted 1:10,000 or anti-rabbit (Sigma-Aldrich; catalog no. A0545), diluted 1:15,000, both conjugated to horseradish peroxidase. Bands were visualized using the Amersham ECL prime Western blotting detection reagent (GE Healthcare; no. RPN2236) and imaged on the Bio-Rad ChemiDoc XRS+ system.

Quantitative PCR of cell-associated RNA. Total RNA was extracted from cells using an RNeasy kit (Qiagen; no. 74106). RNA was DNase treated using the TURBO DNA-free kit (Invitrogen; no. AM1907). cDNA was synthesized using random hexamer primers and SuperScript III first-strand synthesis kit (Invitrogen; no. 18080051). Quantitative PCR (qPCR) was performed using SensiFast SYBR No-ROX kit (Bioline; no. BIO-98020). Samples were run in duplicate or triplicate. The mRNA expression was normalized to RPL13A mRNA expression, and the relative abundance was calculated ($\Delta\Delta C_T$).

qPCR primers. The following RPL13A primer was purchased from Bio-Rad: PrimePCR SYBR green assay RPL13A human no. 10025637. Other primers used were: XPB-F, GGATGAGTCAGGCACCAAAGT; XPB-R, CTGGAGAGAAGGCTTCCAAGAA; XPD-F, CGACTACATCTACCCCGAGCA; XPD-R, CATGATCAGGGCCA ACAGGGA; CCNH-F, TCACCCCAGGATAATAATGCTCA; CCNH-R, CAGTATCTGTTCAAGTGCCTTCT; CDK7-F, GGAGCCCCAATAGAGCTTATACA; CDK7-R, TCCACACCTACACCATACATCC; GTF2H1-F, GACCTTGTTGTGAGT CAAGTGA; GTF2H1-R, CCTGCTTATGATTGGATGTGGAA; GTF2H2-F, CGTATGGGATTTCCTCAGCAC; GTF2H2-R, AGCCTCCTAATGTAAGCCCTG; GTF2H3-F, GAATGGCAGACTTGGAGACTTC; GTF2H3-R, GCAAAGTTTCTGTATG TTGACCC; GTF2H4-F, ACCCCATTTTCCGCCAGAAC; GTF2H4-R, CGGCGTACTTGTCAAGGGAG; GTF2H5-F, AAGACATTGATGACACTCACGTC; GTF2H5-R, GGGAAAAAGCATTTTGGTCCATT; MNAT1-F, GGTTGCCCT CGGTGTAAGAC; MNAT1-R, AGTTGCTCTTTCTGAGTGGAGT; AllHIVmRNA-F, TTGCTCAATGCCACAGCCAT; AllHIVmRNA-R, TTTGACCACTTGCCACCCAT; HIV early *gag*-F, GCGACTGGTGAGTACGCCAA; HIV early *gag*-R, CCCCTGGCCTTAACCGAATTT.

ChIP qPCR primers. 123-F, CCCTGATTGGCAGAACTACACAC; 123-R, TCTACCTTATCTGGCTCAACTGGT; 326-F, GACAGCCGCCTAGCATTTCAT; 326-R, CCACGCCTCCCTGGAAAGT; 412-F, CGAGAGCTGCATCC GGAGTACT; 412-R, GAGGCTTAAGCAGTGGGTTCC; 1097-F, GCAGTCCTCTATTGTGTGCATCAA; 1097-R, CCTGTGTCAGCTGCTGCTTG; 1477-F, CCATCAATGAGGAAGCTGCAGAA; 1477-R, GGTGGATTATGTGT CATCCATCCT; 3582-F, CAGAAATACAGAAGCAGGGGCAA; 3582-R, GTGTGGGCACCCTTCATTCTT; 6352-F, GAGCAGAAGACAGTGGCAATGA; 6352-R, CACAGGTACCCCATAATAGACTGTG; 8885-F, CCTGCTGTAA GGGAAAGAATGAGAC; 8885-R, CACCTCTTCCTCCTCTTGTGCT; GAPDH-F, CCTCACGTATTCCCCCAGGT TTA; GAPDH-R, AGCCACACCATCCTAGTTGCCT.

Cell cycle stage analysis. OM-10.1 cells were treated long-term (80 to 100 days) with ART and 10 μM SP, 10 μM EPL, or DMSO, and they were split and treated every 72 h. After 72 h of incubation, 1×10^6 cells was collected per condition (in triplicate) for cell cycle analysis. All centrifugation steps were performed at 500 $\times$ *g* for 5 min. For fixation, cells were washed in 1$\times$ Dulbecco's phosphate-buffered saline (DPBS) (Gibco; no. 14190-250) and then fixed in 66% ice-cold ethanol, on ice, for at least 2 h or stored at 4°C until the next day. For staining, fixed cells were equilibrated to room temperature, resuspended, and pelleted. Fixing solution was aspirated and cells were washed with 1$\times$ DPBS. The pellet was resuspended in 0.5 ml of FxCycle PI/RNase staining solution (Invitrogen; no. F10797) and stained for 15 to 30 min at room temperature (RT) and protected from light. Cells were acquired on a BD LSR II flow cytometer using the 561-nm laser with the 617/25 band-pass filter.

Transduction of OM-10.1 cells. The Mission shRNAs targeting ERCC3 and GFP in the pLKO.1-puro plasmid were purchased from Sigma-Aldrich (SHCLNG TRCN0000359264 and SHC204, respectively). First, lentiviral vectors were prepared by transient transfection of 293T cells, with the shRNA vector and packaging plasmids pMD2.g and psPAX2 (gifts from Didier Trono; Addgene plasmid no. 12259 and no. 12260) at a molar ratio of 2:1:1, respectively. Transfections were performed using TransIT-LT1 transfection reagent (Mirus Bio LLC; no. MIR 2305) as per manufacturer's instructions. Lentiviral virus-like particles (VLPs) were collected and filtered through a 0.45-μm filter, to remove cellular debris, at 48 and 72 h posttransfection. Filtered VLPs were combined, quantified, and stored at -80°C until use. Three days prior to transduction, medium was changed on OM-10.1 cells to remove ART to allow successful transduction with the VLPs. OM-10.1 cells were transduced with equal multiplicities of infection (MOIs) of lentiviral vectors in T25 flasks as follows: pLKO.1-shGFP, pLKO.1-ERCC3, pLKO.1-shGFP + 1.8 μM SP, and pLKO.1-shGFP + 6.3 μM SP in the presence of the indicated concentrations of SP. VLPs were added to cells and a nontransduced control was included. Cells were washed after an overnight incubation, and ART ($\pm$ the indicated SP concentrations) was added back to the medium. Two days later, cells were selected with 1.5 μg/ml puromycin (Gemini Bio-Products; no. 400-128P). Cells were maintained in

puromycin-supplemented medium treated with the indicated concentrations of SP every 3 days. Ten days post-puromycin selection, cells were harvested for XPB protein analysis by Western blotting and RNA expression analysis of *ERCC3* and HIV by RT-qPCR. Additionally, supernatant was collected from each transduction for quantification of HIV capsid protein by p24 ELISA. Cells were counted, and viability was determined by trypan blue staining using the TC20 automated cell counter.

Latent HIV-1 reactivation. OM-10.1 cells (after 45 days of treatment with ART and 10 μM SP or DMSO) and ACH-2 cells (after 15 days of treatment with ART and 10 μM SP or DMSO) were stimulated (or not) with 1 μM prostratin (LC Laboratories; no. P-4462-1MG), 10 ng/ml TNF-α (BioLegend; no. 570104), 1 μM SAHA (LC Laboratories; no. V-8477_1g), or 20 nM PMA (Sigma-Aldrich; no. P1585-1MG). This was done in the presence of ART and either 10 μM SP or DMSO. After 8 h, p24 production was measured in the supernatant by ELISA, and cells were collected for RNA extraction and RT-qPCR analysis.

J-Lat A1 cells were treated with 160 nM PMA or 1 ng/ml TNF-α for 2 h and then treated overnight with 10 μM SP, EPL, or DMSO, after which the mean fluorescence intensity of GFP was measured by flow cytometry. J-Lat 11.1 cells were treated with 8 nM PMA for 2 h following overnight treatment with 10 μM SP, EPL, or DMSO.

Isolation, expansion, and reactivation of primary CD4$^+$ T cells. Resting CD4$^+$ T cells were isolated from 7 ART-treated, virally suppressed, HIV-1-infected individuals through magnetic negative depletion as previously described (91) and treated with SP (10 μM) or mock (DMSO) for 24 h. The fusion inhibitor enfuvirtide (T20) was supplemented to the cell culture to prevent new rounds of infection. In the final 6 h of culture, the cells were treated with PMA (50 ng/ml) and ionomycin (1 μM) to induce maximum *ex vivo* latency reversal as previously described (64). Cell-associated HIV-1 RNA was extracted using TRIzol phase separation and DNase treatment. HIV-1 RNA expression was measured by RT-qPCR as cell-associated polyadenylated HIV-1 levels per million CD4$^+$ T cells (92, 93). Cellular gene expression (*POLR2A*; Thermo Fisher; no. 4331182) was measured as cell-associated polyadenylated *POLR2A* levels per million CD4$^+$ T cells.

RNA polymerase II ChIP. Three independent treatments of OM-10.1 cells with ART and 10 μM SP or DMSO for ~70 days were stimulated (or not) with 1 μM prostratin for 8 h. Supernatant and cells were collected for p24 ELISA and RT-qPCR analysis, respectively, and remaining cells were cross-linked with 1% formaldehyde for 10 min and quenched by 0.125 M glycine for 5 min at room temperature. Cells were lysed using an SDS lysis buffer, and lysates were sonicated 16 times for 10-s bursts on ice to generate sheared chromatin of 200 to 400 nucleotides in the presence of complete EDTA-free protease inhibitor cocktail (Roche; no. 4693132001) and phosphatase inhibitor cocktail 3 (Sigma-Aldrich; no. P0044-1ML). The protein concentration of the precleared sonicated lysate was determined using the Bradford protein assay. A 4% fraction of each sonicated lysate was reserved for the input control. Four micrograms (per condition) of each of the antibodies total RNAP II (Millipore; no. 05-623), pSer5 RNAPII CTD (Active Motif; no. 61986), and pSer2 RNAPII CTD (Active Motif; no. 61984) or isotype controls mouse IgG (Invitrogen; no. 31903) or rat IgG (Thermo Fisher Scientific; no. 029602) were conjugated to protein G Dynabeads (Thermo Fisher Scientific; no. 10003D) for 20 min, rotating at RT. A total of 500 μg precleared protein lysate was added to the conjugated beads for immunoprecipitation (IP) overnight with rotation at 4°C. Dynabeads were washed using magnetic separation. Samples were then treated (including input samples) with freshly prepared digestion buffer (10 mM Tris-HCl, 1 mM EDTA, 0.5% SDS, 10 μg/ml RNase A [Thermo Scientific; no. EN0531]) at 37°C for 30 min. Cross-links were reversed for at least 4 h shaking (1,000 rpm) at 65°C with 200 nM NaCl. DNA samples were then treated with proteinase K (Fisher Scientific; no. BP1700100) shaking (1,000 rpm) at 60°C for 1 h. Dynabeads were removed, and DNA was purified using the QIAquick PCR purification kit (Qiagen; no. 28106). qPCR was performed in 384-well format using SensiFast SYBR No-ROX kit (Bioline; no. BIO-98020). The average threshold cycle (C_T) value of the IgG-only background for each primer was subtracted from the C_T value using the HIV-1 primer. The data were then normalized to input values using the following formula: % of input = [2-∂C_T(IP) – 2-∂C_T(IgG)] $\times$ 4.

mRNA-seq library preparation. Total RNA was extracted using the RNeasy kit (Qiagen; no. 74106). RNA was DNase treated using the TURBO DNA-free kit (Invitrogen; no. AM1907). Total RNA was quantified on the Qubit 2.0 fluorometer and run on the Agilent 2100 Bioanalyzer RNA pico chip (Agilent Technologies, Santa Clara, CA) for quality assessment. mRNA was selectively isolated from total RNA (500 ng) using poly-T oligonucleotides attached to magnetic beads according to the manufacturer's guidelines in the NEBNext poly(A) mRNA magnetic isolation module (catalog no. E7490; NEB, Ipswich, MA). The library preparation from the enriched mRNA was conducted according to NEBNext Ultra II directional RNA kit (catalog no. E7760; NEB, Ipswich, MA). Briefly, the enriched mRNA samples were chemically fragmented at 94°C for 15 min. The fragmented RNA was random hexamer primed and reverse transcribed to generate the first-strand cDNA. The second strand was synthesized after removing the RNA template and incorporating dUTP in place of dTTP. The incorporation of dUTP quenches the second strand during the PCR amplification step later, and therefore the strand information was preserved. The purified double-stranded (ds) cDNA was end repaired and adenylated at their 3′ ends. A corresponding "T" nucleotide on the adaptors was utilized for ligating the adaptor sequences to the ds cDNA. The adaptor ligated DNA was purified and PCR amplified to incorporate unique barcodes to generate the final libraries. The final libraries were validated on the bioanalyzer DNA chips, pooled equally, and loaded onto the NextSeq 500 for sequencing with 2 $\times$ 80-bp paired-end chemistry.

Read mapping and differential expression analysis. Raw FASTQC files were filtered for read quality using trim-galore version 0.6.1 with the following options: –clip_R1 5 –clip_R2 5 –trim-n –paired (https://www.bioinformatics.babraham.ac.uk/projects/trim_galore/). Trimmed reads were aligned to the human transcriptome (GRCh38v100) with the HIV-1 genome added as an additional chromosome

(REFSEQ release 202). To align transcripts, salmon version 0.14.1 was used with the validateMappings option (94). Aligned transcriptomes were mapped to genes, and differential gene expression was called using tximport version 1.16.1 and DESeq2 version 1.28.1, respectively (95, 96). TPMs were determined using the countsFromAbundance = "lengthScaledTPM" option in tximport. All plots were generated in R. GSEAs were computed from the GSEA app version 4.1.0 using TPMs as counts and publicly available gene sets current as of October 2020 (71). DESeq2 and TPM data can be found in Tables S1 to S5 in the supplemental material.

Statistical analysis. Statistics were performed using GraphPad Prism, and a P value of <0.05 was considered significant for all comparisons. *, $P < 0.05$; **, $P < 0.01$; ***, $P < 0.001$; ****, $P < 0.0001$. Not significant (NS) unless indicated. Data are presented as the mean of the indicated replicates with error bars indicating the standard deviation (SD). The two-tailed t test was used where applicable, and a paired t test was used for reactivation studies to compare stimulated conditions to unstimulated conditions. Comparisons of multiple conditions were performed using a two-way analysis of variance (ANOVA) repeated-measures test (Dunnett or Holm-Sidak).

SUPPLEMENTAL MATERIAL

Supplemental material is available online only.

SUPPLEMENTAL FILE 1, XLSX file, 12.3 MB.

REFERENCES

1. Chun TW, Carruth L, Finzi D, Shen X, DiGiuseppe JA, Taylor H, Hermankova M, Chadwick K, Margolick J, Quinn TC, Kuo YH, Brookmeyer R, Zeiger MA, Barditch-Crovo P, Siliciano RF. 1997. Quantification of latent tissue reservoirs and total body viral load in HIV-1 infection. Nature 387:183–188. https://doi.org/10.1038/387183a0.
2. Chun TW, Stuyver L, Mizell SB, Ehler LA, Mican JAM, Baseler M, Lloyd AL, Nowak MA, Fauci AS. 1997. Presence of an inducible HIV-1 latent reservoir during highly active antiretroviral therapy. Proc Natl Acad Sci U S A 94:13193–13197. https://doi.org/10.1073/pnas.94.24.13193.
3. Finzi D, Hermankova M, Pierson T, Carruth LM, Buck C, Chaisson RE, Quinn TC, Chadwick K, Margolick J, Brookmeyer R, Gallant J, Markowitz M, Ho DD, Richman DD, Siliciano RF. 1997. Identification of a reservoir for HIV-1 in patients on highly active antiretroviral therapy. Science 278:1295–1300. https://doi.org/10.1126/science.278.5341.1295.
4. Wong JK, Hezareh M, Günthard HF, Havlir DV, Ignacio CC, Spina CA, Richman DD. 1997. Recovery of replication-competent HIV despite prolonged suppression of plasma viremia. Science 278:1291–1295. https://doi.org/10.1126/science.278.5341.1291.
5. Darcis G, Van Driessche B, Van Lint C. 2017. HIV latency: should we shock or lock? Trends Immunol 38:217–228. https://doi.org/10.1016/j.it.2016.12.003.
6. Marsden MD, Zack JA. 2019. HIV cure strategies: a complex approach for a complicated viral reservoir? Future Virol 14:5–8. https://doi.org/10.2217/fvl-2018-0205.
7. Pitman MC, Lau JSY, McMahon JH, Lewin SR. 2018. Barriers and strategies to achieve a cure for HIV. Lancet HIV 5:e317–e328. https://doi.org/10.1016/S2352-3018(18)30039-0.
8. Ruelas DS, Greene WC. 2013. An integrated overview of HIV-1 latency. Cell 155:519–529. https://doi.org/10.1016/j.cell.2013.09.044.
9. Sylla L, Evans D, Taylor J, Gilbertson A, Palm D, Auerbach JD, Dubé K. 2018. If we build it, will they come? Perceptions of HIV cure-related research by people living with HIV in four U.S. cities: a qualitative focus group study. AIDS Res Hum Retroviruses 34:56–66. https://doi.org/10.1089/AID.2017.0178.
10. Paiardini M, Müller-Trutwin M. 2013. HIV-associated chronic immune activation. Immunol Rev 254:78–101. https://doi.org/10.1111/imr.12079.
11. Sereti I, Altfeld M. 2016. Immune activation and HIV: an enduring relationship. Curr Opin HIV AIDS 11:129–130. https://doi.org/10.1097/COH.0000000000000244.
12. Klatt NR, Chomont N, Douek DC, Deeks SG. 2013. Immune activation and HIV persistence: implications for curative approaches to HIV infection. Immunol Rev 254:326–342. https://doi.org/10.1111/imr.12065.
13. Olsen HS, Rosen CA. 1992. Contribution of the TATA motif to Tat-mediated transcriptional activation of human immunodeficiency virus gene expression. J Virol 66:5594–5597. https://doi.org/10.1128/JVI.66.9.5594-5597.1992.
14. Compe E, Egly J-M. 2016. Nucleotide excision repair and transcriptional regulation: TFIIH and beyond. Annu Rev Biochem 85:265–290. https://doi.org/10.1146/annurev-biochem-060815-014857.
15. Compe E, Genes CM, Braun C, Coin F, Egly JM. 2019. TFIIE orchestrates the recruitment of the TFIIH kinase module at promoter before release during transcription. Nat Commun 10:2084. https://doi.org/10.1038/s41467-019-10131-1.
16. Yan C, Dodd T, He Y, Tainer JA, Tsutakawa SE, Ivanov I. 2019. Transcription preinitiation complex structure and dynamics provide insight into genetic diseases. Nat Struct Mol Biol 26:397–406. https://doi.org/10.1038/s41594-019-0220-3.
17. Compe E, Egly JM. 2012. TFIIH: when transcription met DNA repair. Nat Rev Mol Cell Biol 13:343–354. https://doi.org/10.1038/nrm3350.
18. Tomko EJ, Fishburn J, Hahn S, Galburt EA. 2017. TFIIH generates a six-base-pair open complex during RNAP II transcription initiation and start-site scanning. Nat Struct Mol Biol 24:1139–1145. https://doi.org/10.1038/nsmb.3500.
19. Greber BJ, Toso DB, Fang J, Nogales E. 2019. The complete structure of the human TFIIH core complex. Elife 8:e44771. https://doi.org/10.7554/eLife.44771.
20. Sandrock B, Egly JM. 2001. A yeast four-hybrid system identifies Cdk-activating kinase as a regulator of the XPD helicase, a subunit of transcription factor IIH. J Biol Chem 276:35328–35333. https://doi.org/10.1074/jbc.M105570200.
21. Coin F, Marinoni JC, Rodolfo C, Fribourg S, Pedrini AM, Egly JM. 1998. Mutations in the XPD helicase gene result in XP and TTD phenotypes, preventing interaction between XPD and the p44 subunit of TFIIH. Nat Genet 20:184–188. https://doi.org/10.1038/2491.
22. Rossignol M, Kolb-Cheynel I, Egly JM. 1997. Substrate specificity of the cdk-activating kinase (CAK) is altered upon association with TFIIH. EMBO J 16:1628–1637. https://doi.org/10.1093/emboj/16.7.1628.
23. Kao SY, Calman AF, Luciw PA, Peterlin BM. 1987. Anti-termination of transcription within the long terminal repeat of HIV-1 by tat gene product. Nature 330:489–493. https://doi.org/10.1038/330489a0.
24. Wada T, Takagi T, Yamaguchi Y, Watanabe D, Handa H. 1998. Evidence that P-TEFb alleviates the negative effect of DSIF on RNA polymerase II-dependent transcription in vitro. EMBO J 17:7395–7403. https://doi.org/10.1093/emboj/17.24.7395.
25. Yamaguchi Y, Takagi T, Wada T, Yano K, Furuya A, Sugimoto S, Hasegawa J, Handa H. 1999. NELF, a multisubunit complex containing RD, cooperates with DSIF to repress RNA polymerase II elongation. Cell 97:41–51. https://doi.org/10.1016/s0092-8674(00)80713-8.
26. Yamaguchi Y, Inukai N, Narita T, Wada T, Handa H. 2002. Evidence that negative elongation factor represses transcription elongation through binding to a DRB sensitivity-inducing factor/RNA polymerase II complex

and RNA. Mol Cell Biol 22:2918–2927. https://doi.org/10.1128/mcb.22.9.2918-2927.2002.
27. Garber ME, Jones KA. 1999. HIV-1 Tat: coping with negative elongation factors. Curr Opin Immunol 11:460–465. https://doi.org/10.1016/S0952-7915(99)80077-6.
28. Peterlin BM, Price DH. 2006. Controlling the elongation phase of transcription with P-TEFb. Mol Cell 23:297–305. https://doi.org/10.1016/j.molcel.2006.06.014.
29. Garber ME, Mayall TP, Suess EM, Meisenhelder J, Thompson NE, Jones KA. 2000. CDK9 autophosphorylation regulates high-affinity binding of the human immunodeficiency virus type 1 Tat-P-TEFb complex to TAR RNA. Mol Cell Biol 20:6958–6969. https://doi.org/10.1128/mcb.20.18.6958-6969.2000.
30. Mbonye U, Wang B, Gokulrangan G, Shi W, Yang S, Karn J. 2018. Cyclin-dependent kinase 7 (CDK7)-mediated phosphorylation of the CDK9 activation loop promotes P-TEFb assembly with Tat and proviral HIV reactivation. J Biol Chem 293:10009–10025. https://doi.org/10.1074/jbc.RA117.001347.
31. Zhu Y, Pe'ery T, Peng J, Ramanathan Y, Marshall N, Marshall T, Amendt B, Mathews MB, Price DH. 1997. Transcription elongation factor P-TEFb is required for HIV-1 Tat transactivation in vitro. Genes Dev 11:2622–2632. https://doi.org/10.1101/gad.11.20.2622.
32. Wei P, Garber ME, Fang SM, Fischer WH, Jones KA. 1998. A novel CDK9-associated C-type cyclin interacts directly with HIV-1 Tat and mediates its high-affinity, loop-specific binding to TAR RNA. Cell 92:451–462. https://doi.org/10.1016/s0092-8674(00)80939-3.
33. Bisgrove DA, Mahmoudi T, Henklein P, Verdin E. 2007. Conserved P-TEFb-interacting domain of BRD4 inhibits HIV transcription. Proc Natl Acad Sci U S A 104:13690–13695. https://doi.org/10.1073/pnas.0705053104.
34. Fujinaga K, Irwin D, Huang Y, Taube R, Kurosu T, Peterlin BM. 2004. Dynamics of human immunodeficiency virus transcription: P-TEFb phosphorylates RD and dissociates negative effectors from the transactivation response element. Mol Cell Biol 24:787–795. https://doi.org/10.1128/mcb.24.2.787-795.2004.
35. Ivanov D, Kwak YT, Guo J, Gaynor RB. 2000. Domains in the SPT5 protein that modulate its transcriptional regulatory properties. Mol Cell Biol 20:2970–2983. https://doi.org/10.1128/mcb.20.9.2970-2983.2000.
36. Dingwall C, Ernberg I, Gait MJ, Green SM, Heaphy S, Karn J, Lowe AD, Singh M, Skinner MA. 1990. HIV-1 tat protein stimulates transcription by binding to a U-rich bulge in the stem of the TAR RNA structure. EMBO J 9:4145–4153. https://doi.org/10.1002/j.1460-2075.1990.tb07637.x.
37. Dingwall C, Ernberg I, Gait MJ, Green SM, Heaphy S, Karn J, Lowe AD, Singh M, Skinner MA, Valerio R. 1989. Human immunodeficiency virus 1 tat protein binds trans-activation-responsive region (TAR) RNA in vitro. Proc Natl Acad Sci U S A 86:6925–6929. https://doi.org/10.1073/pnas.86.18.6925.
38. Marshall NF, Price DH. 1995. Purification of P-TEFb, a transcription factor required for the transition into productive elongation. J Biol Chem 270:12335–12338. https://doi.org/10.1074/jbc.270.21.12335.
39. Razooky BS, Pai A, Aull K, Rouzine IM, Weinberger LS. 2015. A hardwired HIV latency program. Cell 160:990–1001. https://doi.org/10.1016/j.cell.2015.02.009.
40. Mousseau G, Clementz MA, Bakeman WN, Nagarsheth N, Cameron M, Shi J, Baran P, Fromentin R, Chomont N, Valente ST. 2012. An analog of the natural steroidal alkaloid cortistatin A potently suppresses Tat-dependent HIV transcription. Cell Host Microbe 12:97–108. https://doi.org/10.1016/j.chom.2012.05.016.
41. Mousseau G, Kessing CF, Fromentin R, Trautmann L, Chomont N, Valente ST. 2015. The tat inhibitor didehydro-cortistatin a prevents HIV-1 reactivation from latency. mBio 6:e00465-15. https://doi.org/10.1128/mBio.00465-15.
42. Aoki S, Watanabe Y, Sanagawa M, Setiawan A, Kotoku N, Kobayashi M. 2006. Cortistatins A, B, C, and D, anti-angiogenic steroidal alkaloids, from the marine sponge Corticium simplex. J Am Chem Soc 128:3148–3149. https://doi.org/10.1021/ja057404h.
43. Kessing CF, Nixon CC, Li C, Tsai P, Takata H, Mousseau G, Ho PT, Honeycutt JB, Fallahi M, Trautmann L, Garcia JV, Valente ST. 2017. In vivo suppression of HIV rebound by didehydro-cortistatin A, a "block-and-lock" strategy for HIV-1 treatment. Cell Rep 21:600–611. https://doi.org/10.1016/j.celrep.2017.09.080.
44. Li C, Mousseau G, Valente ST. 2019. Tat inhibition by didehydro-cortistatin A promotes heterochromatin formation at the HIV-1 long terminal repeat. Epigenetics Chromatin 12:23. https://doi.org/10.1186/s13072-019-0267-8.
45. Delyani JA. 2000. Mineralocorticoid receptor antagonists: the evolution of utility and pharmacology. Kidney Int 57:1408–1411. https://doi.org/10.1046/j.1523-1755.2000.00983.x.
46. Alekseev S, Ayadi M, Brino L, Egly JM, Larsen AK, Coin F. 2014. A small molecule screen identifies an inhibitor of DNA repair inducing the degradation of TFIIH and the chemosensitization of tumor cells to platinum. Chem Biol 21:398–407. https://doi.org/10.1016/j.chembiol.2013.12.014.
47. Elinoff JM, Chen LY, Dougherty EJ, Awad KS, Wang S, Biancotto A, Siddiqui AH, Weir NA, Cai R, Sun J, Preston IR, Solomon MA, Danner RL. 2018. Spironolactone-induced degradation of the TFIIH core complex XPB subunit suppresses NF-κB and AP-1 signalling. Cardiovasc Res 114:65–76. https://doi.org/10.1093/cvr/cvx198.
48. Lacombe B, Morel M, Margottin-Goguet F, Ramirez BC. 2016. Specific Inhibition of HIV infection by the action of spironolactone in T cells. J Virol 90:10972–10980. https://doi.org/10.1128/JVI.01722-16.
49. Verma D, Thompson J, Swaminathan S. 2016. Spironolactone blocks Epstein–Barr virus production by inhibiting EBV SM protein function. Proc Natl Acad Sci U S A 113:3609–3614. https://doi.org/10.1073/pnas.1523686113.
50. Ueda M, Matsuura K, Kawai H, Wakasugi M, Matsunaga T. 2019. Spironolactone-induced XPB degradation depends on CDK7 kinase and SCF^{FBXL18} E3 ligase. Genes Cells 24:284–296. https://doi.org/10.1111/gtc.12674.
51. Alekseev S, Nagy Z, Sandoz J, Weiss A, Egly JM, Le May N, Coin F. 2017. Transcription without XPB establishes a unified helicase-independent mechanism of promoter opening in eukaryotic gene expression. Mol Cell 65:504–514. https://doi.org/10.1016/j.molcel.2017.01.012.
52. Titov DV, Gilman B, He QL, Bhat S, Low WK, Dang Y, Smeaton M, Demain AL, Miller PS, Kugel JF, Goodrich JA, Liu JO. 2011. XPB, a subunit of TFIIH, is a target of the natural product triptolide. Nat Chem Biol 7:182–188. https://doi.org/10.1038/nchembio.522.
53. Kim YK, Bourgeois CF, Pearson R, Tyagi M, West MJ, Wong J, Wu SY, Chiang CM, Karn J. 2006. Recruitment of TFIIH to the HIV LTR is a rate-limiting step in the emergence of HIV from latency. EMBO J 25:3596–3604. https://doi.org/10.1038/sj.emboj.7601248.
54. Butera ST, Perez VL, Wu BY, Nabel GJ, Folks TM. 1991. Oscillation of the human immunodeficiency virus surface receptor is regulated by the state of viral activation in a CD4+ cell model of chronic infection. J Virol 65:4645–4653. https://doi.org/10.1128/JVI.65.9.4645-4653.1991.
55. Garthwaite SM, McMahon EG. 2004. The evolution of aldosterone antagonists. Mol Cell Endocrinol 217:27–31. https://doi.org/10.1016/j.mce.2003.10.005.
56. Clouse KA, Powell D, Washington I, Poli G, Strebel K, Farrar W, Barstad P, Kovacs J, Fauci AS, Folks TM. 1989. Monokine regulation of human immunodeficiency virus-1 expression in a chronically infected human T cell clone. J Immunol 142:431–438.
57. Folks TM, Clouse KA, Justement J, Rabson A, Duh E, Kehrl JH, Fauci AS. 1989. Tumor necrosis factor α induces expression of human immunodeficiency virus in a chronically infected T-cell clone. Proc Natl Acad Sci U S A 86:2365–2368. https://doi.org/10.1073/pnas.86.7.2365.
58. Cannon P, Kim SH, Ulich C, Kim S. 1994. Analysis of Tat function in human immunodeficiency virus type 1-infected low-level-expression cell lines U1 and ACH-2. J Virol 68:1993–1997. https://doi.org/10.1128/JVI.68.3.1993-1997.1994.
59. Emiliani S, Van Lint C, Fischle W, Paras P, Ott M, Brady J, Verdin E. 1996. A point mutation in the HIV-1 Tat responsive element is associated with postintegration latency. Proc Natl Acad Sci U S A 93:6377–6381. https://doi.org/10.1073/pnas.93.13.6377.
60. Duh EJ, Maury WJ, Folks TM, Fauci AS, Rabson AB. 1989. Tumor necrosis factor α activates human immunodeficiency virus type 1 through induction of nuclear factor binding to the NF-κB sites in the long terminal repeat. Proc Natl Acad Sci U S A 86:5974–5978. https://doi.org/10.1073/pnas.86.15.5974.
61. McKernan LN, Momjian D, Kulkosky J. 2012. Protein kinase C: one pathway towards the eradication of latent HIV-1 reservoirs. Adv Virol 2012:805347. https://doi.org/10.1155/2012/805347.
62. Archin NM, Espeseth A, Parker D, Cheema M, Hazuda D, Margolis DM. 2009. Expression of latent HIV induced by the potent HDAC inhibitor suberoylanilide hydroxamic acid. AIDS Res Hum Retroviruses 25:207–212. https://doi.org/10.1089/aid.2008.0191.
63. Williams SA, Chen LF, Kwon H, Fenard D, Bisgrove D, Verdin E, Greene WC. 2004. Prostratin antagonizes HIV latency by activating NF-κB. J Biol Chem 279:42008–42017. https://doi.org/10.1074/jbc.M402124200.
64. Bullen CK, Laird GM, Durand CM, Siliciano JD, Siliciano RF. 2014. New ex vivo approaches distinguish effective and ineffective single agents for

reversing HIV-1 latency in vivo. Nat Med 20:425–429. https://doi.org/10.1038/nm.3489.
65. Kim JB, Sharp PA. 2001. Positive transcription elongation factor b phosphorylates hSPT5 and RNA polymerase II carboxyl-terminal domain independently of cyclin-dependent kinase-activating kinase. J Biol Chem 276:12317–12323. https://doi.org/10.1074/jbc.M010908200.
66. Bowman EA, Kelly WG. 2014. RNA polymerase II transcription elongation and Pol II CTD Ser2 phosphorylation: a tail of two kinases. Nucleus 5:224–236. https://doi.org/10.4161/nucl.29347.
67. Davidson L, Muniz L, West S. 2014. 3′ end formation of pre-mRNA and phosphorylation of Ser2 on the RNA polymerase II CTD are reciprocally coupled in human cells. Genes Dev 28:342–356. https://doi.org/10.1101/gad.231274.113.
68. Greifenberg AK, Hönig D, Pilarova K, Düster R, Bartholomeeusen K, Bösken CA, Anand K, Blazek D, Geyer M. 2016. Structural and functional analysis of the Cdk13/cyclin K complex. Cell Rep 14:320–331. https://doi.org/10.1016/j.celrep.2015.12.025.
69. Liang K, Gao X, Gilmore JM, Florens L, Washburn MP, Smith E, Shilatifard A. 2015. Characterization of human cyclin-dependent kinase 12 (CDK12) and CDK13 complexes in C-terminal domain phosphorylation, gene transcription, and RNA processing. Mol Cell Biol 35:928–938. https://doi.org/10.1128/MCB.01426-14.
70. Baumli S, Lolli G, Lowe ED, Troiani S, Rusconi L, Bullock AN, Debreczeni JÉ, Knapp S, Johnson LN. 2008. The structure of P-TEFb (CDK9/cyclin T1), its complex with flavopiridol and regulation by phosphorylation. EMBO J 27:1907–1918. https://doi.org/10.1038/emboj.2008.121.
71. Subramanian A, Tamayo P, Mootha VK, Mukherjee S, Ebert BL, Gillette MA, Paulovich A, Pomeroy SL, Golub TR, Lander ES, Mesirov JP. 2005. Gene set enrichment analysis: a knowledge-based approach for interpreting genome-wide expression profiles. Proc Natl Acad Sci U S A 102:15545–15550. https://doi.org/10.1073/pnas.0506580102.
72. Fabregat A, Sidiropoulos K, Garapati P, Gillespie M, Hausmann K, Haw R, Jassal B, Jupe S, Korninger F, McKay S, Matthews L, May B, Milacic M, Rothfels K, Shamovsky V, Webber M, Weiser J, Williams M, Wu G, Stein L, Hermjakob H, D'Eustachio P. 2016. The reactome pathway knowledgebase. Nucleic Acids Res 44:D481–D487. https://doi.org/10.1093/nar/gkv1351.
73. Günesdogan U, Jäckle H, Herzig A. 2014. Histone supply regulates S phase timing and cell cycle progression. Elife 3:e02443. https://doi.org/10.7554/eLife.02443.
74. Egloff S, Murphy S. 2008. Cracking the RNA polymerase II CTD code. Trends Genet 24:280–288. https://doi.org/10.1016/j.tig.2008.03.008.
75. Komarnitsky P, Cho EJ, Buratowski S. 2000. Different phosphorylated forms of RNA polymerase II and associated mRNA processing factors during transcription. Genes Dev 14:2452–2460. https://doi.org/10.1101/gad.824700.
76. Custódio N, Carmo-Fonseca M. 2016. Co-transcriptional splicing and the CTD code. Crit Rev Biochem Mol Biol 51:395–411. https://doi.org/10.1080/10409238.2016.1230086.
77. Bartkowiak B, Liu P, Phatnani HP, Fuda NJ, Cooper JJ, Price DH, Adelman K, Lis JT, Greenleaf AL. 2010. CDK12 is a transcription elongation-associated CTD kinase, the metazoan ortholog of yeast Ctk1. Genes Dev 24:2303–2316. https://doi.org/10.1101/gad.1968210.
78. Yoh SM, Cho H, Pickle L, Evans RM, Jones KA. 2007. The Spt6 SH2 domain binds Ser2-P RNAPII to direct Iws1-dependent mRNA splicing and export. Genes Dev 21:160–174. https://doi.org/10.1101/gad.1503107.
79. Hoeijmakers JHJ, Egly JM, Vermeulen W. 1996. TFIIH: a key component in multiple DNA transactions. Curr Opin Genet Dev 6:26–33. https://doi.org/10.1016/S0959-437X(96)90006-4.
80. Lee AJE, Parsons LM, Quinn LM. 2014. MYC function and regulation in flies: how Drosophila has enlightened MYC cancer biology. AIMS Genet 1:81–98.
81. Zaytseva O, Quinn LM. 2017. Controlling the master: chromatin dynamics at the MYC promoter integrate developmental signaling. Genes (Basel) 8:118–124. https://doi.org/10.3390/genes8040118.
82. Liu J, He L, Collins I, Ge H, Libutti D, Li J, Egly JM, Levens D. 2000. The FBP interacting repressor targets TFIIH to inhibit activated transcription. Mol Cell 5:331–341. https://doi.org/10.1016/s1097-2765(00)80428-1.
83. Liu J, Kouzine F, Nie Z, Chung HJ, Elisha-Feil Z, Weber A, Zhao K, Levens D. 2006. The FUSE/FBP/FIR/TFIIH system is a molecular machine programming a pulse of c-myc expression. EMBO J 25:2119–2130. https://doi.org/10.1038/sj.emboj.7601101.
84. Donnio LM, Miquel C, Vermeulen W, Giglia-Mari G, Mari PO. 2019. Cell-type specific concentration regulation of the basal transcription factor TFIIH in $XPB^{y/y}$ mice model. Cancer Cell Int 19:237. https://doi.org/10.1186/s12935-019-0945-4.
85. Gardiner P, Schrode K, Quinlan D, Martin BK, Boreham DR, Rogers MS, Stubbs K, Smith M, Karim A. 1989. Spironolactone metabolism: steady-state serum levels of the sulfur-containing metabolites. J Clin Pharmacol 29:342–347. https://doi.org/10.1002/j.1552-4604.1989.tb03339.x.
86. Sinclair R, Patel M, Dawson TL, Yazdabadi A, Yip L, Perez A, Rufaut NW. 2011. Hair loss in women: medical and cosmetic approaches to increase scalp hair fullness. Br J Dermatol 165:12–18. https://doi.org/10.1111/j.1365-2133.2011.10630.x.
87. Prior JC, Vigna YM, Watson D. 1989. Spironolactone with physiological female steroids for presurgical therapy of male-to-female transsexualism. Arch Sex Behav 18:49–57. https://doi.org/10.1007/BF01579291.
88. Spark RF, Melby JC. 1968. Aldosteronism in hypertension. The spironolactone response test. Ann Intern Med 69:685–691. https://doi.org/10.7326/0003-4819-69-4-685.
89. Lachaine J, Beauchemin C, Ramos E. 2011. Use, tolerability and compliance of spironolactone in the treatment of heart failure. BMC Clin Pharmacol 11:4. https://doi.org/10.1186/1472-6904-11-4.
90. Mediouni S, Kessing CF, Jablonski JA, Thenin-Houssier S, Clementz M, Kovach MD, Mousseau G, De Vera IMS, Li C, Kojetin DJ, Evans DT, Valente ST. 2019. The Tat inhibitor didehydro-cortistatin A suppresses SIV replication and reactivation. FASEB J 33:8280–8293. https://doi.org/10.1096/fj.201801165R.
91. Ho YC, Shan L, Hosmane NN, Wang J, Laskey SB, Rosenbloom DIS, Lai J, Blankson JN, Siliciano JD, Siliciano RF. 2013. Replication-competent noninduced proviruses in the latent reservoir increase barrier to HIV-1 cure. Cell 155:540–551. https://doi.org/10.1016/j.cell.2013.09.020.
92. Shan L, Rabi SA, Laird GM, Eisele EE, Zhang H, Margolick JB, Siliciano RF. 2013. A novel PCR assay for quantification of HIV-1 RNA. J Virol 87:6521–6525. https://doi.org/10.1128/JVI.00006-13.
93. Pollack RA, Jones RB, Pertea M, Bruner KM, Martin AR, Thomas AS, Capoferri AA, Beg SA, Huang SH, Karandish S, Hao H, Halper-Stromberg E, Yong PC, Kovacs C, Benko E, Siliciano RF, Ho YC. 2017. Defective HIV-1 proviruses are expressed and can be recognized by cytotoxic T lymphocytes, which shape the proviral landscape. Cell Host Microbe 21:494–506. https://doi.org/10.1016/j.chom.2017.03.008.
94. Patro R, Duggal G, Love MI, Irizarry RA, Kingsford C. 2017. Salmon provides fast and bias-aware quantification of transcript expression. Nat Methods 14:417–419. https://doi.org/10.1038/nmeth.4197.
95. Soneson C, Love MI, Robinson MD. 2016. Differential analyses for RNA-seq: transcript-level estimates improve gene-level inferences. F1000Res 4:1521–1523. https://doi.org/10.12688/f1000research.7563.2.
96. Love MI, Huber W, Anders S. 2014. Moderated estimation of fold change and dispersion for RNA-seq data with DESeq2. Genome Biol 15:550. https://doi.org/10.1186/s13059-014-0550-8.